

ITP-SB-96-32  
LBNL-39025

# Resummed heavy quark production cross sections to next-to-leading logarithm

N. Kidonakis and J. Smith<sup>1</sup>

*Institute for Theoretical Physics  
State University of New York at Stony Brook  
Stony Brook, NY 11794-3840*

R. Vogt<sup>2</sup>

*Nuclear Science Division,  
Lawrence Berkeley National Laboratory,  
Berkeley, CA 94720  
and  
Physics Department,  
University of California at Davis  
Davis, CA 95616*

August 1996

## Abstract

We study how next-to-leading logarithms modify predictions from leading logarithmic soft-gluon resummation in the heavy quark production cross section near threshold. Numerical results are presented for top quark production at the Fermilab Tevatron and bottom quark production at fixed-target energies.

---

<sup>1</sup>This work was supported in part under contract NSF 93-09888.

<sup>2</sup>This work was supported in part by the Director, Office of Energy Research, Division of Nuclear Physics of the Office of High Energy and Nuclear Physics of the U. S. Department of Energy under Contract Number DE-AC03-76SF0098.

# 1 Introduction

The calculation of hadronic cross sections in the elastic limit (*i.e.*, near threshold) in perturbative QCD involves contributions from the emission of soft gluons. In  $n$ -th order QCD one encounters leading logarithmic (LL) contributions proportional to  $\alpha_s^n [(-1)^n \ln^{2n+1} (1-z)/(1-z)]_+$ , as well as next-to-leading logarithmic (NLL) contributions proportional to  $\alpha_s^n [(-1)^n \ln^{2n} (1-z)/(1-z)]_+$ . These “plus” distributions are large near threshold,  $z = 1$ , (the precise definition of  $z$  will be given in the next section) and resummation techniques were originally developed to sum them in Drell-Yan production [1]. As the Drell-Yan process involves electroweak interactions it has a rather simple color structure. Gluons are only radiated from the incoming quark-antiquark pair in the hadronic collision process so the amplitude is a color singlet.

The first resummation of LL terms (as well as some NLL terms) in the heavy (top) quark production cross section was discussed [2, 3] prior to the discovery of the top quark at the Fermilab Tevatron [4]. The analysis was based on the fact that the LL terms are identical to those in the Drell-Yan process and, even though a cutoff was used to define the resummed perturbation series, this paper pointed out the importance of incorporating resummation effects in threshold production of heavy quarks in QCD. Recently other groups have applied more sophisticated LL resummation methods to the top quark production cross section, *c.f.* Refs. [5, 6], which avoid the use of an explicit cutoff, and lead to slightly different values for the top quark cross section. At present the experimental results cannot discriminate between them and there is an ongoing discussion as to which method is theoretically superior. The quark-antiquark annihilation channel is the dominant partonic process for top quark production in  $p\bar{p}$  collisions at center of mass energy  $\sqrt{S} = 1.8$  TeV. However the gluon-gluon channel is more important in bottom and charm production near threshold in fixed-target experiments with proton and pion beams. The LL resummation method of [2] has also been applied to  $b$ -quark production at HERA-B [7] and more generally for fixed-target bottom and charm production by hadron beams [8].

The order  $\alpha_s^2$  corrections to the Drell-Yan process in [9] have allowed a check of the NLL terms in the resummation formulae, thus the theory is in excellent shape. However, this information cannot be used in heavy-quark resummation since some of the NLL terms are a consequence of the more

complicated color structure in heavy quark production. There is no exact calculation of the heavy-quark production cross section at order  $\alpha_s^4$ . Even though the NLL terms at order  $\alpha_s^3$  for heavy quark production near threshold were available in 1990 [10], at the time of the heavy quark resummation analysis [2] it was not clear how to resum them. Therefore all work has concentrated on the LL terms. Now this situation has changed. A resummation formalism which correctly incorporates NLL resummation near threshold has recently been presented by Kidonakis and Sterman [11, 12]. The authors analytically compared the order-by-order expansion of their results with the known NLL terms [10] and found agreement at threshold in both the quark-antiquark channel and the gluon-gluon channel.

In this paper we will apply this new NLL resummation formalism to calculate the top quark production cross section at the Fermilab Tevatron and the bottom quark production cross section at fixed target energies. We are particularly interested in the size and therefore the phenomenological importance of the NLL terms with respect to the LL terms. We will use the cutoff method proposed originally in [2]. There are several reasons for this, which we now discuss. First, we are interested in the corrections the NLL terms make to the LL terms and we expect this ratio to be similar for all the resummation methods. Next, by varying the cutoff the failure of the perturbative expansion and the onset of the nonperturbative region may be studied directly, bypassed in the newer methods. Finally, given the complexity of the formulae it is best to use the simplest approach to incorporate the NLL terms in a first test of their magnitude. An analysis of the NLL terms is very important since the present LL resummations are based either on neglecting them entirely or retaining only some of them. Since these terms are not universal, they could be of importance in several areas of perturbative QCD besides the analysis of the heavy quark cross section, including the production of large transverse energy jets and the production of supersymmetric particles. The conclusions of our study should not be generalized to these other reactions since each process is different and requires a separate study.

## 2 General Formalism

Here we present some basic formulae which we need for our analysis. A complete exposition of the theoretical background is available in [11, 12]. For heavy quark production to be kinematically allowed, the square of the partonic center of mass energy,  $s = x_a x_b S$ , must be larger than the threshold value of the invariant mass of the heavy quark-antiquark pair,  $Q^2 = 4m^2$ . When the heavy quarks are produced with zero velocity, the true threshold and the partonic threshold are equivalent. In either case, the plus distributions which must be resummed are functions of

$$z = \frac{Q^2}{s}. \quad (2.1)$$

Our calculations are based on the factorization of soft gluons from high-energy partons in perturbative QCD [13, 14]. All the singular distributions in the heavy quark ( $Q$ ) production cross section can be expressed in the form

$$\begin{aligned} \frac{d\sigma_{h_1 h_2}}{dQ^2 d \cos \theta^* dy} &= \sum_{ab} \sum_{IJ} \int \frac{dx_a}{x_a} \frac{dx_b}{x_b} \phi_{a/h_1}(x_a, Q^2) \phi_{b/h_2}(x_b, Q^2) \\ &\quad \times \delta\left(y - \frac{1}{2} \ln \frac{x_a}{x_b}\right) \hat{\sigma}_{ab}^{(IJ)}\left(\frac{Q^2}{x_a x_b S}, \theta^*, \alpha_s(Q^2)\right), \end{aligned} \quad (2.2)$$

where  $x_a, x_b$  are the momentum fractions of the incoming partons,  $y$  is the rapidity of the  $Q\bar{Q}$  pair, and  $\theta^*$  is the scattering angle in the pair center of mass system. The  $\phi$ 's are parton densities, evaluated at the mass factorization scale  $Q^2$ , in the DIS or  $\overline{\text{MS}}$  scheme. The hard scattering functions  $\hat{\sigma}$ , which depend on the color structure ( $IJ$ ) of the interaction as well as on the partonic channel  $ab$  and the mass factorization scheme ( $\overline{\text{MS}}$  or DIS), contain all the plus distributions in the threshold region. In [11] it was shown that to NLL it is possible to pick a color basis in which moments of the functions  $\hat{\sigma}_{ab}^{(IJ)}(z, \theta^*, \alpha_s(Q^2))$  exponentiate with respect to  $z$  so that

$$\begin{aligned} \tilde{\sigma}_{ab}^{(IJ)}(n, \theta^*, Q^2) &= \int_0^1 dz z^{n-1} \hat{\sigma}_{ab}^{(IJ)}(z, \theta^*, \alpha_s(Q^2)) \\ &= h_I(\theta^*, Q^2) h_J^*(\theta^*, Q^2) e^{E_{IJ}(n, \theta^*, Q^2)}. \end{aligned} \quad (2.3)$$

The hard scattering prefactor is a product of contributions from the amplitude  $h_I$  and its complex conjugate  $h_J^*$ . Therefore  $I$  refers to the decomposition of the hard scattering amplitude into a color basis, *e.g.* into an  $s$ -channel

singlet and octet. The functions  $h_I$  and  $h_J^*$  have no collinear or soft divergences at the partonic threshold since these terms have been factored into the exponent  $E_{IJ}$  in eq. (2.3). The exponential in (2.3), called  $S_{IJ}$  in [11, 12], satisfies a renormalization group equation with an anomalous dimension matrix  $\Gamma_{IJ}$ .

The exponents of eq. (2.3) are given by

$$\begin{aligned} E_{IJ}^{(ab)}(n, \theta^*, Q^2) = & - \int_0^1 dz \frac{z^{n-1} - 1}{1 - z} \\ & \times \left\{ (2 - r) \int_0^z \frac{dy}{1 - y} g_1^{(ab)}[\alpha_s((1 - y)^{2-r}(1 - z)^r Q^2)] + g_2^{(ab)}[\alpha_s((1 - z)Q^2)] \right. \\ & \left. + g_3^{(I)}[\alpha_s((1 - z)^2 Q^2), \theta^*] + g_3^{(J)*}[\alpha_s((1 - z)^2 Q^2), \theta^*] \right\}, \end{aligned} \quad (2.4)$$

where  $g_1$ ,  $g_2$  and  $g_3$  are functions of the running coupling constant  $\alpha_s$  with  $z$ - (and  $y$ )-dependent arguments. The parameter  $r$  is 1 in the DIS scheme and 0 in the  $\overline{\text{MS}}$  scheme. The effect of the parameter is to change the lower limit of the  $y$ -integral in the  $\overline{\text{MS}}$  scheme (*c.f.* [15] and our later discussion). As it stands eq. (2.4) is ill-defined as it incorporates arbitrarily soft gluon radiation where the QCD perturbation expansion diverges. There are different opinions as to how to define it in a way which clearly separates the perturbative region from the non-perturbative region. We will return to this point shortly.

To go to NLL in the exponents  $E_{IJ}$ , we need  $g_1$  up to and including  $O(\alpha_s^2)$  and  $g_2$  and  $g_3^{(I)}$  to  $O(\alpha_s)$ . Refs. [5, 6] treat  $g_1$  to  $O(\alpha_s^2)$  and include  $g_2$  but do not include the NLL  $g_3$  term, treated numerically for the first time here.

The function  $g_1$  is essentially independent of the color structure and only depends on the identity of the incoming partons,

$$g_1^{(ab)}[\alpha_s] = (C_a + C_b) \left( \frac{\alpha_s}{\pi} + \frac{1}{2} K \left( \frac{\alpha_s}{\pi} \right)^2 \right), \quad (2.5)$$

where  $C_q = C_{\bar{q}} = C_F$  and  $C_g = C_A$ . The constant  $K$  is (*c.f.* [16])

$$K = C_A \left( \frac{67}{18} - \frac{\pi^2}{6} \right) - \frac{5}{9} n_f, \quad (2.6)$$

where  $n_f$  is the number of quark flavors.

The  $g_2$  contribution depends on the mass factorization scheme [15]. In the DIS scheme,

$$g_2^{(q\bar{q}) \text{DIS}}[\alpha_s] = -\frac{3}{2} C_F \frac{\alpha_s}{\pi}, \quad (2.7)$$

while in the  $\overline{\text{MS}}$  scheme,  $g_2^{(q\bar{q})\overline{\text{MS}}} = g_2^{gg} = 0$ .

The functions  $g_3^{(I)}$  depend on the color structure in the hard scattering but are mass factorization scheme independent. In [11, 12] it is shown that they are the eigenvalues of the anomalous dimension matrix  $\Gamma_{IJ}$  which appears in the renormalization group equation for the function  $S_{IJ}$ . The precise definition is

$$g_3^{(I)}[\alpha_s((1-z)^2 Q^2), \theta^*] = -\lambda_I[\alpha_s((1-z)^2 Q^2), \theta^*], \quad (2.8)$$

showing that  $g_3^{(I)}$  and  $\lambda_I$  are functions of both the running coupling constant  $\alpha_s$  (evaluated at a  $z$ -dependent scale) and the angle  $\theta^*$  between the directions of the incoming and outgoing partons. Note that although the eigenvalues are complex, the total  $g_3$  contribution to  $E_{IJ}^{(ab)}$  in eq. (2.4) is real.

Consider first the reaction channel  $q(p_a) + \bar{q}(p_b) \rightarrow \overline{Q}(p_i) + Q(p_j)$  where  $\Gamma_{IJ}$  is two-dimensional. In the  $s$ -channel singlet-octet basis the color decomposition is into  $\delta^{ab}\delta^{ij}$  (singlet) and  $-\delta^{ab}\delta^{ij}/(2N) + \delta^{aj}\delta^{bi}/2$  (octet). In this basis the components of the matrix  $\Gamma_{IJ}$  are [12]

$$\begin{aligned} \Gamma_{11} &= -\frac{\alpha_s}{\pi} C_F (L_\beta + 1 + i\pi), \\ \Gamma_{21} &= \frac{2\alpha_s}{\pi} \ln\left(\frac{u_1}{t_1}\right), \\ \Gamma_{12} &= \frac{\alpha_s}{\pi} \frac{C_F}{C_A} \ln\left(\frac{u_1}{t_1}\right), \\ \Gamma_{22} &= \frac{\alpha_s}{\pi} \left\{ C_F \left[ 4 \ln\left(\frac{u_1}{t_1}\right) - L_\beta - 1 - i\pi \right] \right. \\ &\quad \left. + \frac{C_A}{2} \left[ -3 \ln\left(\frac{u_1}{t_1}\right) - \ln\left(\frac{m^2 s}{t_1 u_1}\right) + L_\beta + i\pi \right] \right\}. \end{aligned} \quad (2.9)$$

where

$$L_\beta = \frac{1 - 2m^2/s}{\beta} \left[ \ln\left(\frac{1 - \beta}{1 + \beta}\right) + i\pi \right], \quad (2.10)$$

and  $\beta^2 = 1 - 4m^2/s$ . The Mandelstam invariants for the reaction are  $s = (p_a + p_b)^2$ ,  $t = t_1 + m^2 = (p_a - p_i)^2$ , and  $u = u_1 + m^2 = (p_b - p_i)^2$ .

$\Gamma_{IJ}$  is diagonalized in this basis when the parton-parton c.m. scattering angle  $\theta^* = 90^\circ$  ( $u_1 = t_1 = -s/2$  at threshold) with eigenvalues

$$\lambda_1 = \lambda_{\text{singlet}} = -\frac{\alpha_s}{\pi} C_F (L_\beta + 1 + i\pi), \quad (2.11)$$

$$\lambda_2 = \lambda_{\text{octet}} = \frac{\alpha_s}{\pi} \left\{ -C_F(L_\beta + 1 + i\pi) + \frac{C_A}{2} \left[ L_\beta - \ln \left( \frac{m^2 s}{t_1^2} \right) + i\pi \right] \right\}.$$

It is also diagonalized at partonic threshold  $s = 4m^2$  for arbitrary  $\theta^*$ .

In the partonic channel  $g(p_a) + g(p_b) \rightarrow Q(p_i) + \bar{Q}(p_j)$  the anomalous dimension matrix is three dimensional. In the color basis  $\delta^{ab} \delta_{ij}, d^{abc} T_{ij}^c$  and  $if^{abc} T_{ij}^c$  the components of the matrix  $\Gamma_{IJ}$  are [12]

$$\begin{aligned} \Gamma_{11} &= -\frac{\alpha_s}{\pi} [C_F(L_\beta + 1) + C_A i\pi], \\ \Gamma_{21} &= 0, \\ \Gamma_{31} &= -\frac{2\alpha_s}{\pi} \ln \left( \frac{u_1}{t_1} \right), \\ \Gamma_{12} &= 0, \\ \Gamma_{22} &= \frac{\alpha_s}{\pi} \left\{ -C_F(L_\beta + 1) + \frac{C_A}{2} \left[ -\ln \left( \frac{m^2 s}{t_1 u_1} \right) + L_\beta - i\pi \right] \right\}, \\ \Gamma_{32} &= \frac{N^2 - 4}{4N} \Gamma_{31}, \\ \Gamma_{13} &= \frac{1}{2} \Gamma_{31}, \\ \Gamma_{23} &= \frac{C_A}{4} \Gamma_{31}, \\ \Gamma_{33} &= \Gamma_{22}. \end{aligned} \tag{2.12}$$

At  $\theta^* = 90^\circ$  the anomalous dimension matrix becomes diagonal with eigenvalues

$$\begin{aligned} \lambda_1 &= -\frac{\alpha_s}{\pi} [C_F(L_\beta + 1) + C_A i\pi], \\ \lambda_2 &= \frac{\alpha_s}{\pi} \left\{ -C_F(L_\beta + 1) + \frac{C_A}{2} \left[ L_\beta - \ln \left( \frac{m^2 s}{t_1^2} \right) - i\pi \right] \right\}, \\ \lambda_3 &= \lambda_2. \end{aligned} \tag{2.13}$$

We note that  $\Gamma_{IJ}$  is also diagonal at partonic threshold for arbitrary  $\theta^*$ .

### 3 Heavy-quark production cross sections

We are primarily interested in the magnitude of the NLL terms, particularly the  $g_3$  contribution, relative to the LL results of [2, 3, 7, 8]. In principle this

requires three separate studies as each group redefines eq. (2.4) differently. However we anticipate that the corrections due to the NLL terms within one scheme are representative of what happens in all schemes so we choose the simplest approach. Therefore we use a cutoff scheme which avoids working in Mellin space, and modify the definitions of the exponents in eqs. (2.3) and (2.4) to work directly in momentum space. This is the method introduced in [2] which exploited the correspondence between the moment variable  $n$  and logarithmic terms in the momentum space variable  $1 - z$ .

First, we identify

$$1 - z = \frac{s_4}{2m^2}, \quad (3.1)$$

where  $s_4$  is the invariant mass of the heavy-quark + gluon system which recoils against the detected heavy antiquark in inclusive  $\overline{Q}$  production. The invariants satisfy  $s + t_1 + u_1 = s_4$  so that in the elastic limit  $s_4 \rightarrow 0$  or  $z \rightarrow 1$ . Note that eq. (3.1) differs from the identification  $1 - z = s_4/m^2$  in Refs. [2, 5]. The factor of two is necessary to compare the NLL terms [12] with the previously given NLL expressions [10]. With the identification in eq. (3.1) all the NLL terms in the  $q\overline{q}$  channel are reproduced, not only exactly at threshold but also at finite  $s_4$  except for one NLL term in  $C_F^2$  which has a different coefficient. (This agreement was unexpected as the  $Q\overline{Q}$  invariant mass and the  $Qg$  invariant mass are different invariants). A similar observation holds for the  $gg$  channel.

Further we exploit the fact that a heavy quark-antiquark pair will be preferentially produced back-to-back in the parton-parton center-of-mass frame near threshold. Therefore we also take to  $\theta^* = 90^\circ$  to use the results of eqs. (2.11) and (2.13). This choice avoids both the diagonalization of the three dimensional matrix in the gluon-gluon channel and an extra numerical integration over  $\theta^*$ .

The resummation is done using eqs. (3.17) and (3.19) of [2] where the “plus” distributions are removed through integration by parts. Therefore we use the formula for the resummed cross section

$$\sigma_{ab}(s, m^2) = - \int_0^{s-2ms^{1/2}} ds_4 f_{ab} \left( \frac{s_4}{2m^2} \right) \frac{d\sigma_{ab}^{(0)}(s, s_4, m^2)}{ds_4}, \quad (3.2)$$

where  $ab = q\overline{q}$  or  $gg$ . The two inputs needed here are the function  $f_{ab}$ , in either the DIS scheme or the  $\overline{MS}$  scheme and the differential of the Born

cross section. Note that  $\alpha_s$  in eqs. (2.5)-(2.11) is a function of  $s_4/2m^2$ . The renormalization group is used to evolve  $\alpha_s$  to other scales. The exponential function  $f_{ab}(s_4/2m^2)$  is given by a momentum space version of eq. (2.4). Using the above mentioned correspondence we replace the numerator,  $z^{n-1} - 1$ , by  $-1$  and introduce the variables  $\omega = 1 - z = s_4/(2m^2)$  and  $\xi = (1 - y)(1 - z)m^2/\Lambda^2$ .

We first discuss the  $q\bar{q}$  channel. There is only one kinematic structure in this channel so that the singlet and octet eigenvalues in eq. (2.11) multiply the same function. At this order in perturbation theory however, only the octet component contributes, *c.f.* the discussion in [11]. Therefore in the DIS scheme at  $\theta^* = 90^\circ$ , the exponential function is

$$f_{q\bar{q}}^{\text{DIS}}\left(\frac{s_4}{2m^2}\right) = \exp[E_{q\bar{q}}^{\text{DIS}} + E_{q\bar{q}}(\lambda_2)], \quad (3.3)$$

where

$$\begin{aligned} E_{q\bar{q}}^{\text{DIS}} &= E_{q\bar{q}}^{\text{DIS}}(g_1) + E_{q\bar{q}}^{\text{DIS}}(g_2) \\ &= \int_{\omega_0}^1 \frac{d\omega}{\omega} \left\{ \int_{\omega^2 m^2 / \Lambda^2}^{\omega m^2 / \Lambda^2} \frac{d\xi}{\xi} \left[ \frac{2C_F}{\pi} \left( \alpha_s(\xi) + \frac{1}{2\pi} \alpha_s^2(\xi) K \right) \right. \right. \\ &\quad \left. \left. - \frac{3}{2} \frac{C_F}{\pi} \alpha_s \left( \frac{\omega m^2}{\Lambda^2} \right) \right] \right\}. \end{aligned} \quad (3.4)$$

Since our calculation is not done in moment space, the  $\omega$  integral is cut off at  $\omega_0 = s_{\text{cut}}/2m^2$ . Because the running coupling constant diverges, the minimum cutoff is  $s_{\text{cut}} = s_{4,\text{min}} \sim 2\Lambda^2$ . In general we choose a larger value. Once we have chosen a reasonable cutoff, consistent with the sum of the first few terms in the perturbative expansion, we can study the size of the NLL terms with respect to the LL terms (the order-by-order expansion does not require a cutoff).

We use the two-loop running coupling constant,

$$\begin{aligned} \alpha_s(\xi) &= \frac{1}{a \ln \xi} + \frac{b \ln(\ln \xi)}{a \ln^2(\xi)}, \\ a &= \frac{11C_A - 4T_f n_f}{12\pi}, \\ b &= -6 \frac{17C_A^2 - (6C_F + 10C_A)T_f n_f}{(11C_A - 4T_f n_f)^2}, \end{aligned} \quad (3.5)$$

with  $C_A = 3$ ,  $C_F = 4/3$  and  $T_f = 1/2$ . It is obvious that when  $\xi < 1$ ,  $\ln \xi$  is negative so that  $\ln(\ln \xi)$  has a cut and needs a precise definition. We use the cutoff on the  $\omega$  variable to stop the integration at that point. The exact cutoff depends on the quark mass and  $\Lambda_{nf}$  in the parton densities. The  $\xi$  integral over  $\alpha_s(\xi)$  and  $\alpha_s^2(\xi)$  in eq. (3.4) can be done analytically.

In the  $\overline{\text{MS}}$  scheme,

$$f_{q\bar{q}}^{\overline{\text{MS}}} \left( \frac{s_4}{2m^2} \right) = \exp[E_{q\bar{q}}^{\overline{\text{MS}}} + E_{q\bar{q}}(\lambda_2)], \quad (3.6)$$

where now

$$E_{q\bar{q}}^{\overline{\text{MS}}} = E_{q\bar{q}}(g_1) = \int_{\omega_0}^1 \frac{d\omega}{\omega} \int_{\omega^2 m^2 / \Lambda^2}^{m^2 / \Lambda^2} \frac{d\xi}{\xi} \left[ \frac{2C_F}{\pi} \left( \alpha_s(\xi) + \frac{1}{2\pi} \alpha_s^2(\xi) K \right) \right]. \quad (3.7)$$

Note the difference between the upper limits of the  $\xi$ -integrations in eqs. (3.4) and (3.7).

The color-dependent  $g_3$  contribution in eq. (2.11) leads to

$$E_{q\bar{q}}(\lambda_i) = - \int_{\omega_0}^1 \frac{d\omega}{\omega} \left\{ \lambda_i \left[ \alpha_s \left( \frac{\omega^2 m^2}{\Lambda^2} \right), \theta^* = 90^\circ \right] + \lambda_i^* \left[ \alpha_s \left( \frac{\omega^2 m^2}{\Lambda^2} \right), \theta^* = 90^\circ \right] \right\}. \quad (3.8)$$

in both mass factorization schemes, where  $i = 1, 2$ .

The differential function in eq. (3.2) follows from the kinematic behaviour of the Born cross section, represented by

$$F_{q\bar{q}}^B(s, t_1, u_1) = \frac{t_1^2 + u_1^2}{s^2} + \frac{2m^2}{s}. \quad (3.9)$$

Substituting  $t_1 = -1/2\{s - s_4 - [(s - s_4)^2 - 4sm^2]^{1/2} \cos \theta^*\}$  and  $u_1 = -1/2\{s - s_4 + [(s - s_4)^2 - 4sm^2]^{1/2} \cos \theta^*\}$ , and taking  $\theta^* = 90^\circ$ , we define, analogous to eq. (2.20) in [2]

$$\overline{F}_{q\bar{q}}^{(0)} = \frac{[(s - s_4)^2 - 4sm^2]^{1/2}}{2s^2} F_{q\bar{q}}^B. \quad (3.10)$$

Differentiating with respect to  $s_4$ , we find

$$\frac{d\overline{F}_{q\bar{q}}^{(0)}}{ds_4} = -\frac{1}{4s^4} \frac{s - s_4}{\sqrt{(s - s_4)^2 - 4sm^2}} [3(s - s_4)^2 - 4sm^2]. \quad (3.11)$$

The integrand in eq. (3.2) becomes, for both factorization schemes,

$$f_{q\bar{q}} \left( \frac{s_4}{2m^2} \right) \frac{d\bar{\sigma}_{q\bar{q}}^{(0)}(s, s_4, m^2)}{ds_4} = \pi \alpha_s^2(m^2) K_{q\bar{q}} N C_F \frac{d\bar{F}_{q\bar{q}}^{(0)}}{ds_4} \times \exp[E_{q\bar{q}} + E_{q\bar{q}}(\lambda_2)], \quad (3.12)$$

where  $K_{q\bar{q}} = 1/N^2$  is a color average factor. We note that near threshold  $d\bar{\sigma}_{q\bar{q}}^{(0)}/ds_4$  is approximately a factor of two smaller than  $d\sigma_{q\bar{q}}^{(0)}/ds_4$  in eq. (3.20) of Ref. [2] where the angle  $\theta^*$  was analytically integrated before differentiating with respect to  $s_4$ .

The treatment of the gluon-gluon channel is very similar but now we have three distinct color structures. However, at  $\theta^* = 90^\circ$  only two of them are independent. Therefore we define  $f_{gg}$  for each eigenvalue so that  $f_{gg,i} = \exp(E_{gg} + E_{gg}(\lambda_i))$  with a one-to-one correspondence between  $E_{gg}(\lambda_i)$  and the eigenvalues of eq. (2.13) so that

$$E_{gg}(\lambda_i) = - \int_{\omega_0}^1 \frac{d\omega}{\omega} \left\{ \lambda_i \left[ \alpha_s \left( \frac{\omega^2 m^2}{\Lambda^2} \right), \theta^* = 90^\circ \right] + \lambda_i^* \left[ \alpha_s \left( \frac{\omega^2 m^2}{\Lambda^2} \right), \theta^* = 90^\circ \right] \right\}, \quad (3.13)$$

where  $i = 1, 2$ . In the  $\overline{\text{MS}}$  scheme,

$$E_{gg} = \int_{\omega_0}^1 \frac{d\omega}{\omega} \int_{\omega^2 m^2 / \Lambda^2}^{m^2 / \Lambda^2} \frac{d\xi}{\xi} \left[ \frac{2C_A}{\pi} \left( \alpha_s(\xi) + \frac{1}{2\pi} \alpha_s^2(\xi) K \right) \right], \quad (3.14)$$

where  $K$  is defined as in eq. (2.6). This identification requires some justification which we have not found explicitly in the literature. However, it should be possible to prove rigorously [17].

Because there are two kinematical structures,  $d\bar{\sigma}_{gg}^{(0)}/ds_4$  has two contributions:

$$\begin{aligned} F_{gg,I}^B(s, t_1, u_1) &= \frac{t_1}{u_1} + \frac{u_1}{t_1} + \frac{4m^2 s}{t_1 u_1} \left( 1 - \frac{m^2 s}{t_1 u_1} \right) \\ F_{gg,II}^B(s, t_1, u_1) &= \left( 1 - \frac{4t_1 u_1}{s^2} \right) F_{gg,I}^B(s, t_1, u_1). \end{aligned} \quad (3.15)$$

The second kinematical structure, proportional to the first, comes from the nonabelian part of the cross section. As in eq. (3.10), we define

$$\bar{F}_{gg,i}^{(0)} = \frac{[(s - s_4)^2 - 4sm^2]^{1/2}}{2s^2} F_{gg,i}^B. \quad (3.16)$$

The differential with respect to  $s_4$  of the two components yields

$$\begin{aligned} \frac{d\bar{F}_{gg,I}^{(0)}(s, s_4, m^2)}{ds_4} &= -\frac{1}{2s^2\sqrt{(s-s_4)^2-4sm^2}} \left[ 2(s-s_4) - \frac{16m^2s}{s-s_4} \right. \\ &\quad \left. + \frac{320m^4s^2}{(s-s_4)^3} - \frac{1024m^6s^3}{(s-s_4)^5} \right] \end{aligned} \quad (3.17)$$

$$\begin{aligned} \frac{d\bar{F}_{gg,II}^{(0)}(s, s_4, m^2)}{ds_4} &= \frac{d\bar{F}_{gg,I}^{(0)}(s, s_4, m^2)}{ds_4} \\ &\quad - \frac{1}{2s^2\sqrt{(s-s_4)^2-4sm^2}} \left[ \frac{512m^6s}{(s-s_4)^3} - \frac{6(s-s_4)^3}{s^2} - \frac{64m^4}{s-s_4} \right] \end{aligned} \quad (3.18)$$

Inserting the remaining color factors yields the  $gg$  integrand in eq. (3.2).

$$\begin{aligned} f_{gg}\left(\frac{s_4}{2m^2}\right) \frac{d\bar{\sigma}_{gg}^{(0)}(s, s_4, m^2)}{ds_4} &= \frac{\pi}{4} K_{gg} N C_F \alpha_s^2 \left\{ \left[ 2C_F f_{gg,1}\left(\frac{s_4}{2m^2}\right) \right. \right. \\ &\quad \left. \left. + C_F(N^2-4) f_{gg,2}\left(\frac{s_4}{2m^2}\right) \right] \frac{d\bar{F}_{gg,I}^{(0)}}{ds_4} + 4C_A f_{gg,2}\left(\frac{s_4}{2m^2}\right) \frac{d\bar{F}_{gg,II}^{(0)}}{ds_4} \right\}, \end{aligned} \quad (3.19)$$

where  $K_{gg} = (N^2 - 1)^{-2}$  is a color average factor. One can numerically compare the coefficients of the color terms in  $d\bar{\sigma}_{gg}^{(0)}/ds_4$  in eq. (3.21) of Ref. [2] with the color terms near threshold in  $d\bar{\sigma}_{gg}^{(0)}/ds_4$  in eq. (3.19). Those in Ref. [2] are integrated over the angle  $\theta^*$  before differentiation with respect to  $s_4$  and are several times larger than those found here. Note that eq. (3.19) contains several terms which can have different signs, making it a more complicated function of  $s_4$ . Therefore we do not expect our  $gg$  results to agree with results obtained without attention to the color decomposition [2, 3, 7, 8].

Because the  $\omega$  integral is cut off at  $s_{\text{cut}}$ , the partonic cross section in eq. (3.2) must also have a lower limit of  $s_{\text{cut}}$  for the integrals to be finite. In earlier work up to LL [2, 3, 7, 8], the lower limit of the partonic cross section,  $s_0$ , was taken to be  $s_0/m^2 = (\mu_0/\mu)^2$  in the DIS scheme and  $s_0/m^2 = (\mu_0/\mu)^3$  in the  $\overline{\text{MS}}$  scheme where  $\Lambda \ll \mu_0 \ll \mu$ . It was assumed that the integral over the nonperturbative region below  $s_0$  was negligible compared to the integral over the perturbative region. A stable cross section was obtained by comparing the resummed cross section with the approximate cross section

order by order in perturbation theory up to  $O(\alpha_s^4)$ . The scale  $\mu_0$  was chosen where the resummed and approximate cross sections were compatible. It was found that for  $\mu = m$  in the DIS scheme  $\mu_0 \approx (0.05 - 0.1)m$ . Larger values were needed in the  $\overline{\text{MS}}$  scheme because of the cubic power of  $\mu_0/\mu$ . In the  $q\bar{q}$  channel,  $\mu_0 \approx (0.1 - 0.2)m$ , while  $\mu_0 \approx 0.35m$  in the  $gg$  channel. The  $\mu_0$  needed in the  $gg$  channel was larger because of the color factor  $C_A$  in  $E_{gg}$ , see eq. (3.14). As before, we will use the cutoff method since increasing  $s_{\text{cut}}$  away from  $s_{4,\text{min}}$  stabilizes the resummed perturbative QCD cross section, as shown previously [2, 3].

## 4 Numerical results

We first present our results for top quark production. In fig. 1(a) we plot the exponents contributing to  $f_{q\bar{q}}^{\text{DIS}}$  at  $\theta^* = 90^\circ$  as a function of  $s_4/2m^2$  with  $m = 175 \text{ GeV}/c^2$  and  $\sqrt{s} = 351 \text{ GeV}$ . Since only the octet component contributes to  $g_3$  here, only  $E_{q\bar{q}}(\lambda_2)$  is shown. We also show, for comparison, the one-loop calculation of  $g_1$ ,  $E^{\text{DIS}}$ , given in [2]. The one-loop and two-loop results are quite similar until  $s_4$  approaches  $s_{\text{cut}}$ . As  $\omega m/\Lambda \rightarrow 1$ ,  $E_{q\bar{q}}^{\text{DIS}}(g_1)$  is larger since  $E^{\text{DIS}}$  was smoothed near the cutoff [2]. The sum  $E_{q\bar{q}}^{\text{DIS}}(g_1) + E_{q\bar{q}}(\lambda_2)$  is always larger than  $E^{\text{DIS}}$  because the  $g_3$  contribution compensates for the small, negative  $g_2$  component ( $|E_{q\bar{q}}^{\text{DIS}}(g_2)|$  is shown). The power of  $1 - z$  in  $\alpha_s$  determines the slope of the exponents at small  $s_4/2m^2$ . The  $g_2$  contribution, linear in  $1 - z$ , is the flattest as  $s_4/2m^2 \rightarrow 0$ . The  $g_1$  component shows more growth, diverging from  $E^{\text{DIS}}$  near  $s_{\text{cut}}$ , and the  $g_3$  contribution, quadratic in  $1 - z$ , grows fastest. The growth of the sum is intermediate to that of  $E_{q\bar{q}}^{\text{DIS}}(g_1)$  and  $E_{q\bar{q}}(\lambda_2)$ .

To better illustrate the importance of these contributions to the partonic cross section, we show the relative enhancements as a function of  $s_4/2m^2$  in fig. 1(b). The negative contribution and the slow growth of  $g_2$  near the cutoff are reflected in the near threshold behavior of  $f_{q\bar{q}}(g_1 + g_2)/f_{q\bar{q}}(g_1)$ . Indeed, in the intermediate range of  $s_4/2m^2$ ,  $E^{\text{DIS}}$  is larger than  $E_{q\bar{q}}^{\text{DIS}}(g_1)$ . Although  $E_{q\bar{q}}(\lambda_2)$  dominates  $f_{q\bar{q}}$  as  $s_4/2m^2 \rightarrow 1$ , the enhancement in this region is not very significant. Thus the choice of the cutoff determines the importance of the NLL contributions. However, a large NLL correction is not necessarily reflected in the hadronic cross section since it is the parton luminosity relative to the equivalent  $\eta = s/4m^2 - 1$  that determines the true

strength of the corrections.

Similar results are seen for the exponents in the  $\overline{\text{MS}}$  scheme, shown in fig. 2. The  $g_2$  term vanishes in this scheme. The change in the limit of the  $\xi$  integral increases the phase space of  $E_{q\bar{q}}^{\overline{\text{MS}}}(g_1)$ . Both these changes enhance the  $\overline{\text{MS}}$  result. The  $g_3$  contribution is identical to that shown in fig. 1.

In fig. 3 we plot the corresponding results for the  $gg$  channel in the  $\overline{\text{MS}}$  scheme. Note that the real parts of the  $\lambda_i$ 's are the same in eqs. (2.12) and (2.15) so that the strength of the  $g_3$  contributions are the same in the  $q\bar{q}$  and  $gg$  channels. However, since different color structures in the  $gg$  channel multiply different derivatives of the Born cross section, there is no single sum involving the NLL components as in the  $q\bar{q}$  channel. The  $E_{gg}(\lambda_1)$  component is quite small and negative near threshold, making the sum  $E_{gg} + E_{gg}(\lambda_1)$  indistinguishable from  $E_{gg}$ . The  $E_{gg}(\lambda_2)$  contribution is the same as in the  $q\bar{q}$  channel, resulting in the larger sum  $E_{gg} + E_{gg}(\lambda_2)$  shown in the dot-dashed curve.

We have checked the energy dependence of the  $g_3$  contributions. We find that  $E_{gg}(\lambda_1)$  is always negative, decreasing the NLL correction for all  $s$ . Its energy dependence is quite strong and thus above threshold it serves to damp the resummation. On the other hand, there is very little energy dependence of  $E_{IJ}(\lambda_2)$  close to threshold. As  $s$  grows large, the  $\ln(m^2 s/t_1^2)$  term in eqs. (2.11) and (2.13) dominates the energy dependence, causing  $E_{IJ}(\lambda_2)$  to change sign, eventually leading to a strong damping of the NLL component (and probably leading to a smooth energy variation of the resummed cross section above threshold). This logarithmic term also has the only explicit  $s_4$  dependence of the  $g_3$  contribution at  $\theta^* = 90^\circ$  apart from the argument of  $\alpha_s$ . Since  $\lambda_1$  only depends on  $s_4$  through  $\alpha_s$ , these contributions have similar behaviour in  $s$ .

In fig. 4 we plot the partonic  $t\bar{t}$  cross section as a function of  $\eta$  for the  $q\bar{q}$  and  $gg$  channels. At  $\eta \approx 1$  the  $gg$  contribution is numerically smaller than the corresponding  $q\bar{q}$  result. Because  $d\bar{F}_{gg,II}^{(0)}/ds_4$  is generally opposite in sign to  $d\bar{F}_{gg,I}^{(0)}/ds_4$ , when it grows larger than  $d\bar{F}_{gg,I}^{(0)}/ds_4$  the partonic  $gg$  cross section becomes negative. In our calculation of the hadronic cross section, we exclude this negative region as it is not near threshold.

The importance of the NLL contributions to the partonic cross section depends on the lower limit of the  $s_4$  integral. In fig. 4(a), we have allowed the  $s_4$  integration to proceed to almost  $s_{4,\min}$ , leading to the rather dramatic

rise of the partonic cross section near small  $\eta$ . This particular cutoff is much smaller than the one used previously and therefore unrealistic. Increasing  $s_{\text{cut}}$  to  $10s_{4,\text{min}}$  dramatically slows the growth at  $\eta$  values near the cutoff, as shown in fig. 4(b), particularly for the  $gg$  channel. Increasing  $s_{\text{cut}}$  also has the effect of increasing the minimum  $\eta$ , as noted by the different scales on the  $x$ -axes of figs. 4(a) and 4(b). Around  $\eta \approx 1$ , the  $q\bar{q}$  results are nearly independent of the cutoff. Note that the oscillations at very small  $\eta$  reflect the varying components in (3.12) and (3.19). Note also that the  $gg$  contribution is positive at  $\eta \approx 1$  with the larger cutoff, presumably because the enhancement of  $f_{gg,2}$  with respect to  $f_{gg,1}$  is smaller in this case, see fig. 3(b) and eq. (3.19), reducing the relative strength of  $d\bar{F}_{gg,II}^{(0)}/ds_4$ . To illustrate the contribution of the NLL terms to the partonic cross section, in fig. 4(c) we show the partonic cross section with only the  $g_1$  (and, in the DIS case,  $g_2$ ) contributions for the same value of  $s_{\text{cut}}$ . At  $\eta > 1$  the  $q\bar{q}$  contributions with and without the NLL components are nearly the same but at lower values of  $\eta$  the  $g_3$  contribution makes the partonic cross section up to a factor of two larger. The  $gg$  channel is similar although the different color structure of the NLL terms leads to a stronger variation over all  $\eta$  in this channel.

To summarize the discussion of the partonic cross sections, the results in fig. 4 imply that the relative importance of the NLL contributions to the hadronic cross section depend on which regions in  $\eta$  are weighted most heavily by the convolution with the parton densities. If this turns out to be the region near  $\eta \approx 0.5$ , then we expect the  $gg$  contribution to be comparable to that of the  $q\bar{q}$  channel. If it is the region near  $\eta \approx 2$  then we expect the opposite conclusion. Recalling previous results [2, 3] is not useful since they were obtained by integrating over the angle  $\theta^*$ , whereas here we work at fixed  $\theta^*$ . Note again that the parton luminosity in the  $x$  space probed by the hadronic cross section determines the ultimate importance of the NLL contribution. At the Tevatron energy,  $\sqrt{S} = 1.8$  TeV, and  $m = 175$  GeV/ $c^2$ , typical  $x$  values in the central region are  $x \approx 0.2$ , corresponding to  $\eta_{\text{max}} = 26$ , although when  $\theta^*$  was integrated over, it was found that the region near  $\eta \approx 3$  was the most important (*c.f.* fig.1 in [3]). Finally we note that previously [2, 3, 7, 8] different cutoffs were chosen in the  $q\bar{q}$  and  $gg$  channels to match the order-by-order contributions.

The hadronic cross section calculated to NLL is

$$\sigma^{\text{NLL}}(S, m^2) = \sum_{ij} \int_{\tau_0}^1 d\tau \int_{\tau}^1 \frac{dx}{x} f_i^{h_1}(x, \mu^2) f_j^{h_2}(\frac{\tau}{x}, \mu^2) \sigma_{ij}(\tau S, m^2), \quad (4.1)$$

where  $\sigma_{ij}(\tau S, m^2)$  is the partonic cross section, eq. (3.2) and  $\tau_0 = (m + \sqrt{m^2 + s_{\text{cut}}})^2/S$ . We evaluate the parton densities at  $\mu = m$ . Note that the parton densities are only available to NLO and LL so that the application to a resummed cross section introduces some uncertainty. We have used the MRS D-' DIS densities with  $\Lambda_5 = 0.1559$  GeV for the  $q\bar{q}$  DIS channel and the MRS D-'  $\overline{\text{MS}}$  densities [18, 19] for both channels in this scheme<sup>3</sup>. The result is not strongly dependent on the parton distributions in the  $x$  range probed at this energy, entering primarily through the value of  $\Lambda_5$  since a different set of parton densities have a different  $\Lambda_5$ , changing  $s_{4,\text{min}}$  as well as the value of  $\alpha_s$  entering the exponents. Taking  $\alpha_s$  to only one loop, as in [2], would also increase the exponents and thus the hadronic cross section. For a more complete discussion of the parton density and  $\alpha_s$  dependence, see [8].

In fig. 5(a) we plot the  $t\bar{t}$  production cross section as a function of top quark mass at the Fermilab Tevatron in the DIS and  $\overline{\text{MS}}$  schemes for the  $q\bar{q}$  channel and the  $\overline{\text{MS}}$  scheme for  $gg$  with  $s_{\text{cut}} = 10s_{4,\text{min}}$ . If we would take  $s_{\text{cut}} \approx s_{4,\text{min}}$ , then the cross section will be much larger and the gluon contribution would dominate since at  $s_{\text{cut}} \approx s_{4,\text{min}}$ ,  $\mu_0 \approx 0.0013m$  in the DIS scheme and  $0.002m$  in the  $\overline{\text{MS}}$  scheme. Such a result with a low cutoff is not too surprising, see *e.g.* figs. 12-14 in [2]. The total  $\overline{\text{MS}}$  cross section is 5.5 pb at  $m = 175$  GeV/ $c^2$ , similar to the results of Ref. [5]. We can also infer that the important region in the partonic cross section, shown in fig. 4, is  $\eta \approx 0.5$ . In this region the  $q\bar{q}$  cross section is smaller in the DIS scheme than in the  $\overline{\text{MS}}$ . The  $gg$  and  $\overline{\text{MS}}$   $q\bar{q}$  contributions are comparable.

To quantify the enhancement in the  $t\bar{t}$  cross section due to the NLL terms, in fig. 5(b) we show our results with  $s_{\text{cut}} = 10s_{4,\text{min}}$  and with the NLL contributions excluded, *i.e.* no  $g_3$  component. The NLL contribution becomes larger for larger top mass at this energy. The DIS cross section is enhanced between 20 and 24% as the top mass increases from 140 to 200 GeV/ $c^2$ . The enhancement is somewhat larger for the  $\overline{\text{MS}}$  scheme, between 24 and 29% in the  $q\bar{q}$  channel and 24 to 32% in the  $gg$  channel. The change in the amount of enhancement is, in part, due to the energy dependence of the

---

<sup>3</sup>The  $x$  dependence of the parton densities in the two schemes is very similar.

$g_3$  contribution. For our choice of  $s_{\text{cut}}$ , the  $t\bar{t}$  cross section at  $m = 175 \text{ GeV}/c^2$  without the NLL  $g_3$  contribution is 4 pb. Thus the NLL terms enhance the total  $\overline{\text{MS}}$  cross section by 27% at this mass in our calculation.

We conclude by noting that the scheme dependence is rather strong, especially when  $s_{\text{cut}}$  is close to  $s_{4,\text{min}}$ . The scheme dependence arises because  $f_{q\bar{q}}^{\overline{\text{MS}}} > f_{q\bar{q}}^{\text{DIS}}$ , particularly near  $s_{4,\text{min}}$ , see figs. 1 and 2 and also *e.g.* figs. 12 and 13 in Ref. [2]. At  $m = 175 \text{ GeV}/c^2$  with  $s_{\text{cut}} \approx s_{4,\text{min}}$ , the  $q\bar{q}$  cross section in the  $\overline{\text{MS}}$  scheme is 11 pb while the DIS cross section is about 3 pb, a factor of four difference. Only the  $q\bar{q}$  DIS results were presented in Ref. [3]. Our DIS result is compatible with theirs at  $\mu = m$ . A comparison of the  $q\bar{q}$  results in the DIS and  $\overline{\text{MS}}$  schemes for the improved cross sections with  $m = 100 \text{ GeV}/c^2$  at  $\mu_0 = 0.1m$  in Ref. [2] shows a factor of two difference between the schemes at this mass with  $\mu = m$ . Increasing  $s_{\text{cut}}$  reduces the scheme dependence. At  $s_{\text{cut}} = 10s_{4,\text{min}}$ , the DIS cross section decreases to 2.2 pb while the  $\overline{\text{MS}}$  cross section decreases to 3.6 pb, a stronger drop. For our chosen  $s_{\text{cut}}$ , the  $\overline{\text{MS}}$  cross section is 35-40% larger than the DIS cross section at NLL. The scheme dependence increases slightly with mass at fixed energy. There is no way to reduce the scheme dependence until new sets of parton densities which have incorporated resummation effects before being fitted to data are available. In the absence of such densities we favor the  $\overline{\text{MS}}$  results as they have a more reliable theoretical basis and the  $q\bar{q}$  and  $gg$  channels can be handled consistently.

Since  $\alpha_s$  depends strongly on the heavy quark mass scale, in figs. 6-9 we repeat our calculations for bottom quark production with  $m = 4.75 \text{ GeV}/c^2$  at  $\sqrt{s} = 9.51 \text{ GeV}$ . The smaller quark mass and the larger  $\Lambda_4$  result in a reduced range in  $s_4/2m^2$  before the exponents diverge. The exponents tend to be somewhat smaller for the bottom quark except near  $s_{4,\text{min}}$ . We note that the energy dependence of  $g_3$  is stronger for the lighter quark mass. While  $E_{gg}(\lambda_1)$  is smaller near threshold, it increases faster with energy than at the top quark mass. The shape of the top and bottom quark exponents as  $s_4 \rightarrow s_{4,\text{min}}$  reflects the faster running of the coupling constant for the lighter bottom mass. The sensitivity to  $s_{\text{cut}}$  is stronger than for top production, see [7, 8]. In this case  $s_{\text{cut}} \approx s_{4,\text{min}}$ , shown in fig. 9(a) for the partonic cross sections, corresponds to  $\mu_0 \approx 0.064m$  in the DIS scheme and  $0.095m$  in the  $\overline{\text{MS}}$  scheme. We also show results with  $s_{\text{cut}} = 2s_{4,\text{min}}$ ,  $\mu_0 \approx 0.13m$  and  $0.19m$  in the DIS and  $\overline{\text{MS}}$  schemes, similar to those in [7, 8], with and without the

NLL  $g_3$  terms in fig. 9(b) and 9(c). We have varied  $s_{\text{cut}}$  around this value ( $s_{\text{cut}} = 1.5s_{4,\text{min}}$  and  $2.5s_{4,\text{min}}$ ) and found that for  $\eta < 1$ , the partonic cross section can change by an order of magnitude near  $\eta \sim 0.1$  and a factor of two to three at  $\eta \sim 0.5$ . The largest variation is in the  $gg$  channel. Of course the  $x$  range probed at a given energy again determines the sensitivity of the hadronic cross section. At higher energies, away from threshold, the sensitivity to  $s_{\text{cut}}$  increases. Similar trends can be seen in charm production although for  $c\bar{c}$  production,  $s_{4,\text{min}}$  already corresponds to the  $\mu_0$  values used in [8], suggesting that a stable cross section is even more difficult to obtain for charm production.

In fig. 10 we plot the  $b\bar{b}$  production cross section as a function of beam momentum for  $pp$  interactions with  $s_{\text{cut}} \approx 2s_{4,\text{min}}$ , with and without the NLL  $g_3$  contributions. As expected,  $gg$  fusion is dominant [7, 8]. These energies,  $20 \leq \sqrt{S} \leq 45$  GeV, correspond to  $3.4 \leq \eta_{\text{max}} \leq 24$ . At the HERA-B energy,  $\sqrt{S} = 39$  GeV, we find a total  $\overline{\text{MS}}$  cross section of 3.1 nb without the NLL terms and 4 nb with the NLL terms, a 22% enhancement. The NLL enhancement generally decreases with energy. In the DIS scheme, the  $q\bar{q}$  enhancement decreases from 39 to 25% between  $200 < p_{\text{lab}} < 800$  GeV/c while in the  $\overline{\text{MS}}$  scheme, the enhancement decreases from 42 to 29% in the same energy range. The enhancement in the  $gg$  channel is generally smaller, decreasing from 36 to 20% over these energies, perhaps due to the interplay of the stronger energy dependence of the  $\lambda_1$  and  $\lambda_2$  eigenvalues for the lighter quarks. Above the HERA-B energy, the enhancement increases again. We believe this is due to the interplay of the NLL energy dependence and the cutoff. Therefore the results are quite sensitive to the chosen cutoff, even more than for the top quark. Our results with  $s_{\text{cut}} = 1.5s_{4,\text{min}}$  predict a production cross section of 49 nb at the same energy. Increasing  $s_{\text{cut}}$  reduces the scheme dependence. At  $s_{\text{cut}} = 1.5s_{4,\text{min}}$ , the average difference between the  $q\bar{q}$  results in the two schemes is 46% while at  $s_{\text{cut}} = 2s_{4,\text{min}}$ , the difference decreases to 29%. There seems to be a general increase of the scheme dependence with energy for the bottom quarks. It is difficult to fairly compare the scheme dependence of top and bottom production since the cutoffs do not correspond to the same  $\mu_0$ , as was found earlier [7, 8]. Thus our bottom quark results are illustrative only. However, they clearly indicate that a full calculation including all angles is needed to clarify the resummation for  $b\bar{b}$  production.

## 5 Conclusions

We have investigated the numerical importance of the NLL terms in the resummation of subleading soft gluon contributions near threshold for heavy quark production cross sections. We have shown that these contributions are generally quite small for top production either because they are numerically small or due to cancellations between them. Although this result has only been demonstrated for the resummation method of [2] and at  $\theta^* = 90^\circ$ , it should also hold for other resummation methods [5, 6] and other angles. Thus the top quark cross sections found there will be essentially unchanged by the inclusion of the NLL terms, increasing by less than 30%. Bottom production is much more sensitive to  $s_{\text{cut}}$ , making definitive statements about the resummed cross sections more difficult, particularly in a model without a calculable perturbative cutoff.

We would like to thank G. Sterman and E. Laenen for helpful discussions. R. Vogt and N. Kidonakis would like to thank Brookhaven National Laboratory for hospitality. R. Vogt also thanks SUNY at Stony Brook for hospitality.

## References

- [1] G. Sterman, Nucl. Phys. **B281**, 310 (1987); S. Catani and L. Trentadue, Nucl. Phys. **B327**, 323 (1989).
- [2] E. Laenen, J. Smith, and W.L. van Neerven, Nucl. Phys. **B369**, 543 (1992).
- [3] E. Laenen, J. Smith, and W.L. van Neerven, Phys. Lett. **B321**, 254 (1994).
- [4] F. Abe *et al.*, CDF collaboration., Phys. Rev. Lett. **74**, 2626 (1995); S. Abachi *et al.*, D0 collaboration, Phys. Rev. Lett. **74**, 2632 (1995).
- [5] E.L. Berger and H. Contopanagos, Phys. Lett. **B361**, 115 (1995); ANL-HEP-PR-95-82, hep-ph/9603326; ANL-HEP-CP-96-51, hep-ph/9606421.

- [6] S. Catani, M.L. Mangano, P. Nason, and L. Trentadue, CERN-TH-96-86, hep-ph/9604351.
- [7] N. Kidonakis and J. Smith, Mod. Phys. Lett. **A11**, 587 (1996).
- [8] J. Smith and R. Vogt, LBL-38282, ITP-SB-95-60.
- [9] W.L. van Neerven and E.B. Zijlstra, Nucl. Phys. **B382**, 11 (1992); T. Matsura, R. Hamburg and W.L. van Neerven, Nucl. Phys. **B359**, 343 (1991).
- [10] R. Meng, G.A. Schuler, J. Smith and W.L. van Neerven, Nucl. Phys. **B339**, 325 (1990).
- [11] N. Kidonakis and G. Sterman, ITP-SB-96-7, hep-ph/9604234.
- [12] N. Kidonakis, SUNY at Stony Brook Ph.D. Thesis (1996), hep-ph/9606474.
- [13] J.C. Collins, D.E. Soper and G. Sterman, in *Perturbative Quantum Chrodynamics*, ed. A.H. Mueller (World Scientific, Singapore, 1989), p. 1.
- [14] J.G.M. Gatheral, Phys. Lett. **B133**, 90 (1983); J.C. Collins, in *Perturbative Quantum Chrodynamics*, ed. A.H. Mueller (World Scientific, Singapore, 1989), p. 573.
- [15] H. Contopanagos, E. Laenen and G. Sterman, hep-ph/9604313.
- [16] J. Kodaira and L. Trentadue, Phys. Lett. **B112**, 66 (1982).
- [17] G. Sterman, private communication.
- [18] A.D. Martin, R.G. Roberts, and W.J. Stirling, Phys. Lett. **B306**, 145 (1993).
- [19] H. Plothow-Besch, ‘PDFLIB: Nucleon, Pion and Photon Parton Density Functions and  $\alpha_s$  Calculations’, Users’s Manual - Version 4.16, W5051 PDFLIB, 1994.01.11, CERN-PPE; Comp. Phys. Comm. **75**, 396 (1993).

### Figure Captions

Figure 1. (a) We show the contributions to  $f_{q\bar{q}}^{\text{DIS}}$  in top quark production for  $m = 175 \text{ GeV}/c^2$  and  $\sqrt{s} = 351 \text{ GeV}$  as a function of  $s_4/2m^2$ . The solid curve shows  $\ln(f_{q\bar{q}}^{\text{DIS}})$  for the octet component at  $90^\circ$ , the dot-dashed curve,  $E_{q\bar{q}}(\lambda_2)$ , the dashed curve,  $E_{q\bar{q}}^{\text{DIS}}(g_1)$ , and the dot-dot-dashed curve,  $|E_{q\bar{q}}^{\text{DIS}}(g_2)|$ . The dotted curve shows  $E^{\text{DIS}}$  as defined in eq. (3.30) of Ref. [2]. (b) The ratios of the exponential factors are given to show the enhancement relative to  $f_{q\bar{q}}(g_1) \equiv \exp(E_{q\bar{q}}^{\text{DIS}}(g_1))$ . The solid curve shows  $f_{q\bar{q}}/f_{q\bar{q}}(g_1)$ , the dashed curve,  $f_{q\bar{q}}(g_1 + g_2)/f_{q\bar{q}}(g_1)$ , and the dotted curve,  $f_{q\bar{q}}(g_1 + g_3(\lambda_2))/f_{q\bar{q}}(g_1)$ . The ratio  $f_{q\bar{q}}(g_1)/\exp(E^{\text{DIS}})$ , given in the dot-dashed curve, shows the enhancement of  $g_1$  from eq. (2.5) relative to the one-loop value in [2].

Figure 2. (a) We show the contributions to  $f_{q\bar{q}}^{\overline{\text{MS}}}$  in top quark production for  $m = 175 \text{ GeV}/c^2$  and  $\sqrt{s} = 351 \text{ GeV}$  as a function of  $s_4/2m^2$ . The solid curve shows  $\ln(f_{q\bar{q}})$  for the octet component at  $90^\circ$ , the dot-dashed curve,  $E_{q\bar{q}}(\lambda_2)$ , and the dashed curve,  $E_{q\bar{q}}^{\overline{\text{MS}}}(g_1)$ . The dotted curve shows  $E^{\overline{\text{MS}}}$  as defined in eq. (3.36) of Ref. [2]. (b) The ratios of the exponential factors are given to show the enhancements. The solid curve shows  $f_{q\bar{q}}/f_{q\bar{q}}(g_1)$  while the dashed curve is the ratio  $f_{q\bar{q}}(g_1)/\exp(E^{\overline{\text{MS}}})$ .

Figure 3. (a) We show the contributions to  $f_{gg}$  in top quark production for  $m = 175 \text{ GeV}/c^2$  and  $\sqrt{s} = 351 \text{ GeV}$  as a function of  $s_4/2m^2$ . The solid curve shows  $E_{gg}$ ; the dashed and dotted curves give the contributions from the eigenvalues,  $E_{gg}(\lambda_2)$  and  $|E_{gg}(\lambda_1)|$  respectively. The dot-dashed curve shows the sum  $E_{gg} + E_{gg}(\lambda_2)$ ; the sum  $E_{gg} + E_{gg}(\lambda_1)$  is indistinguishable from the solid curve. The dot-dot-dashed curve shows  $E^{\overline{\text{MS}}}$  for the gluon from Ref. [2]. (b) The ratios of the exponential factors are given to show the enhancements relative to  $f_{gg}(g_1) \equiv \exp(E_{gg})$ . The solid curve shows  $f_{gg}(g_1 + g_3(\lambda_1))/f_{gg}(g_1)$  and the dashed curve,  $f_{gg}(g_1 + g_3(\lambda_2))/f_{gg}(g_1)$ . The ratio of  $f_{gg}(g_1)$  to  $\exp(E^{\overline{\text{MS}}})$ , given in the dot-dashed curve, compares the  $g_1$  from eq. (2.5) relative to the one-loop value in [2].

Figure 4. The partonic top quark production cross section is shown as a function of  $\eta$  for the  $q\bar{q}$  channel in the DIS (solid) and  $\overline{\text{MS}}$  (dashed) schemes and the  $gg$  (dot-dashed) channel. In (a) we show the result with  $s_{\text{cut}} \approx s_{4,\text{min}}$  while (b) and (c) show  $s_{\text{cut}} \approx 10s_{4,\text{min}}$  with and without the NLL  $g_3$  contributions respectively.

Figure 5. The hadronic  $t\bar{t}$  production cross section is given as a function of top quark mass for  $p\bar{p}$  collisions at the Tevatron energy,  $\sqrt{S} = 1.8$  TeV. We use the MRS D-’ parton densities in the DIS scheme for  $q\bar{q}$  annihilation (dashed) and in the  $\overline{\text{MS}}$  scheme for the  $q\bar{q}$  (dot-dashed) and  $gg$  (dotted) channels. The sum of the  $q\bar{q}$  and  $gg$  channels in the  $\overline{\text{MS}}$  scheme is given in the solid curve. The results are given for  $s_{\text{cut}} \approx 10s_{4,\text{min}}$  with the NLL  $g_3$  contributions in (a) and with these excluded in (b).

Figure 6. We show the contributions to  $f_{q\bar{q}}^{\text{DIS}}$  and the enhancement factors in bottom quark production for  $m = 4.75 \text{ GeV}/c^2$  and  $\sqrt{s} = 9.51 \text{ GeV}$ . The labels are as in fig. 1.

Figure 7. We show the contributions to  $f_{q\bar{q}}^{\overline{\text{MS}}}$  and the enhancement factors in bottom quark production for  $m = 4.75 \text{ GeV}/c^2$  and  $\sqrt{s} = 9.51 \text{ GeV}$ . The labels are as in fig. 2.

Figure 8. We show the contributions to  $f_{gg}$  and the enhancement factors in bottom quark production for  $m = 4.75 \text{ GeV}/c^2$  and  $\sqrt{s} = 9.51 \text{ GeV}$ . The labels are as in fig. 3.

Figure 9. The partonic bottom quark production cross section is shown as a function of  $\eta$ . The labels are as in fig. 4. In (a) we show the result with  $s_{\text{cut}} \approx s_{4,\text{min}}$  while  $s_{\text{cut}} = 2s_{4,\text{min}}$  is shown in (b) with the NLL  $g_3$  contributions and in (c) without them.

Figure 10. The hadronic  $b\bar{b}$  production cross section is given as a function of

beam momentum for  $pp$  interactions. We use the MRS D-’ parton densities in the DIS scheme for  $q\bar{q}$  annihilation (dashed) and in the  $\overline{\text{MS}}$  scheme for the  $q\bar{q}$  (dot-dashed) and  $gg$  (dotted) channels. The  $\overline{\text{MS}}$  sum is given in the solid curve. The result are shown with  $s_{\text{cut}} \approx 2s_{4,\text{min}}$  with the NLL  $g_3$  corrections in (a) and without them in (b).

Figure 1

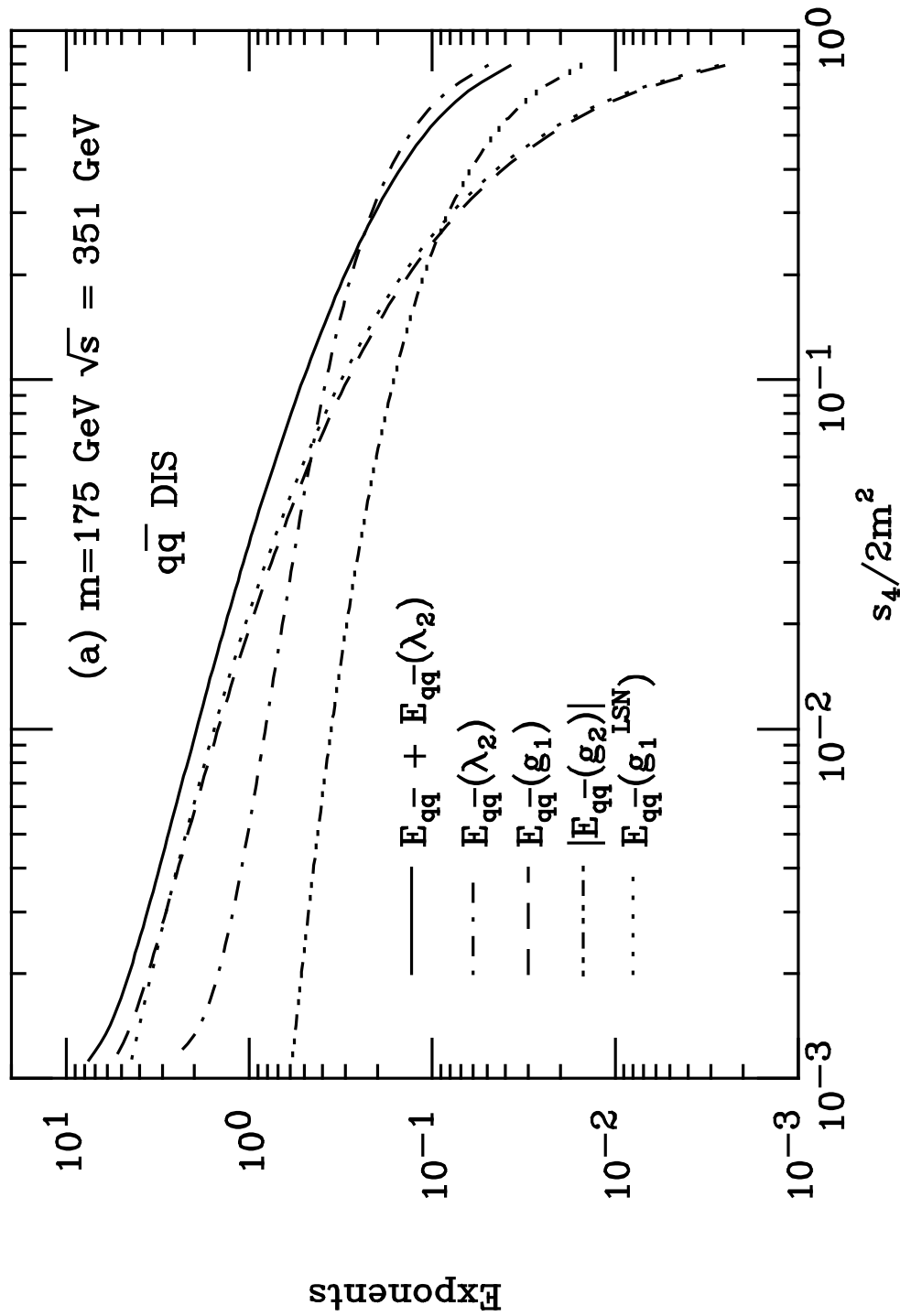


Figure 1

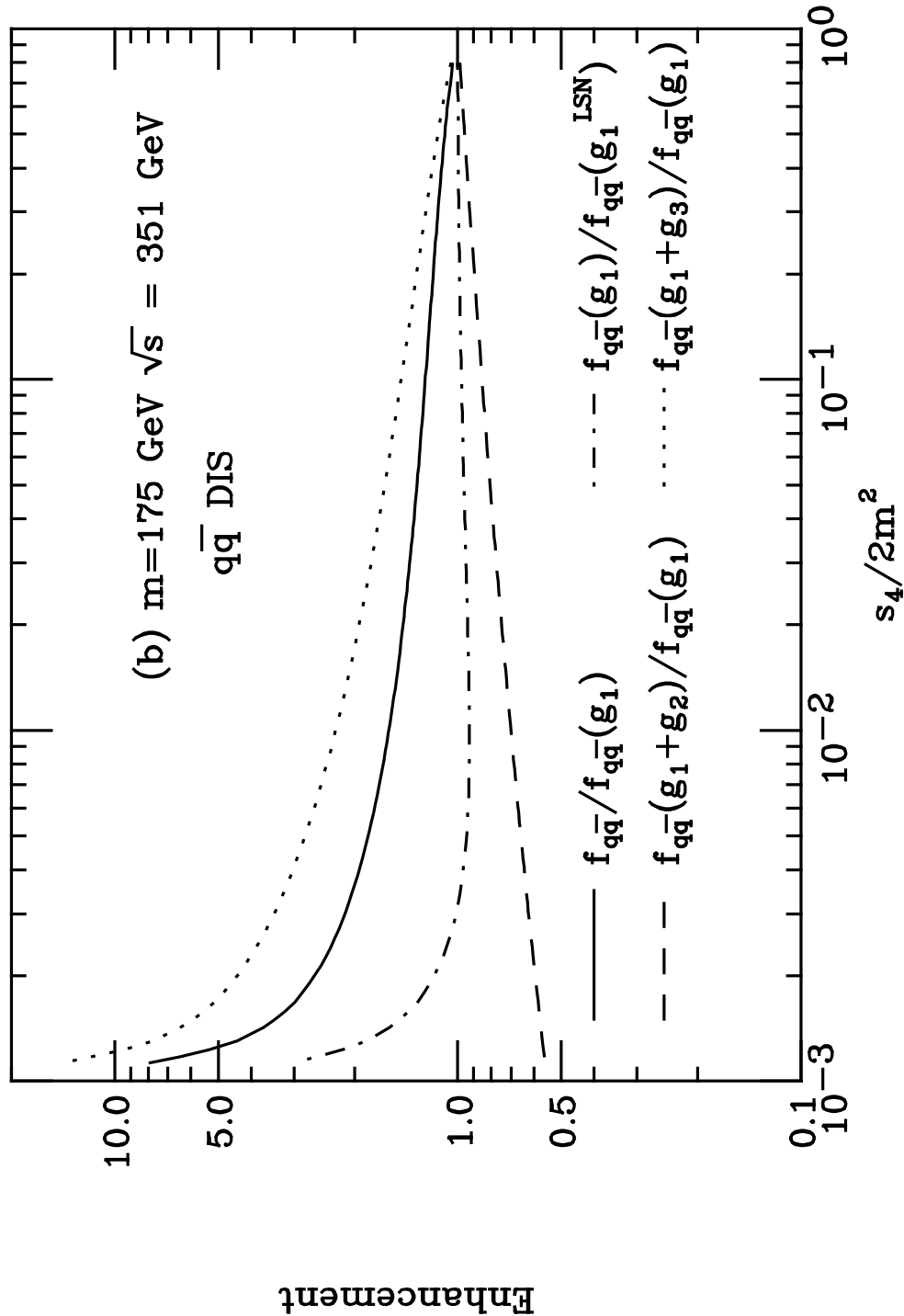


Figure 2

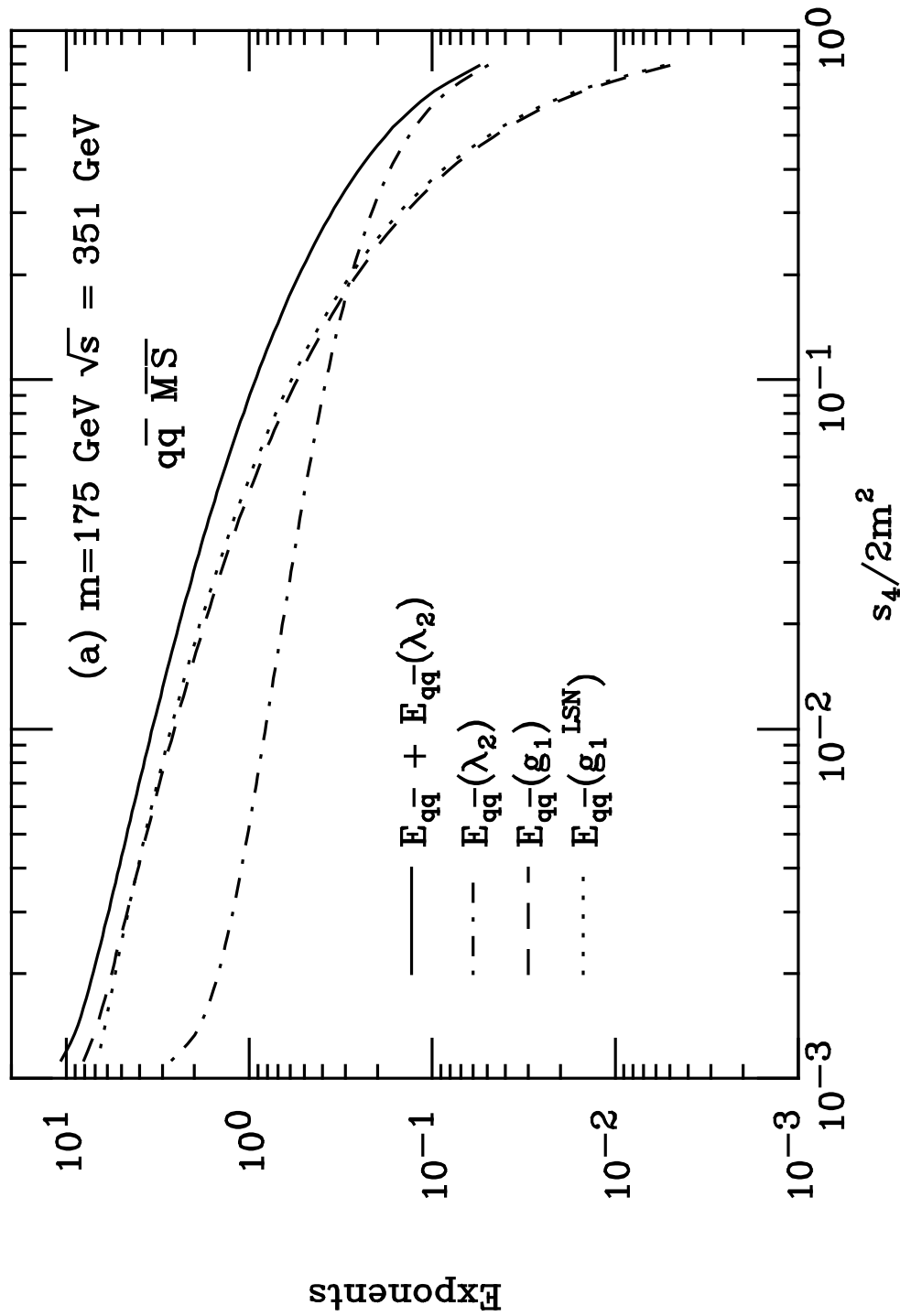


Figure 2

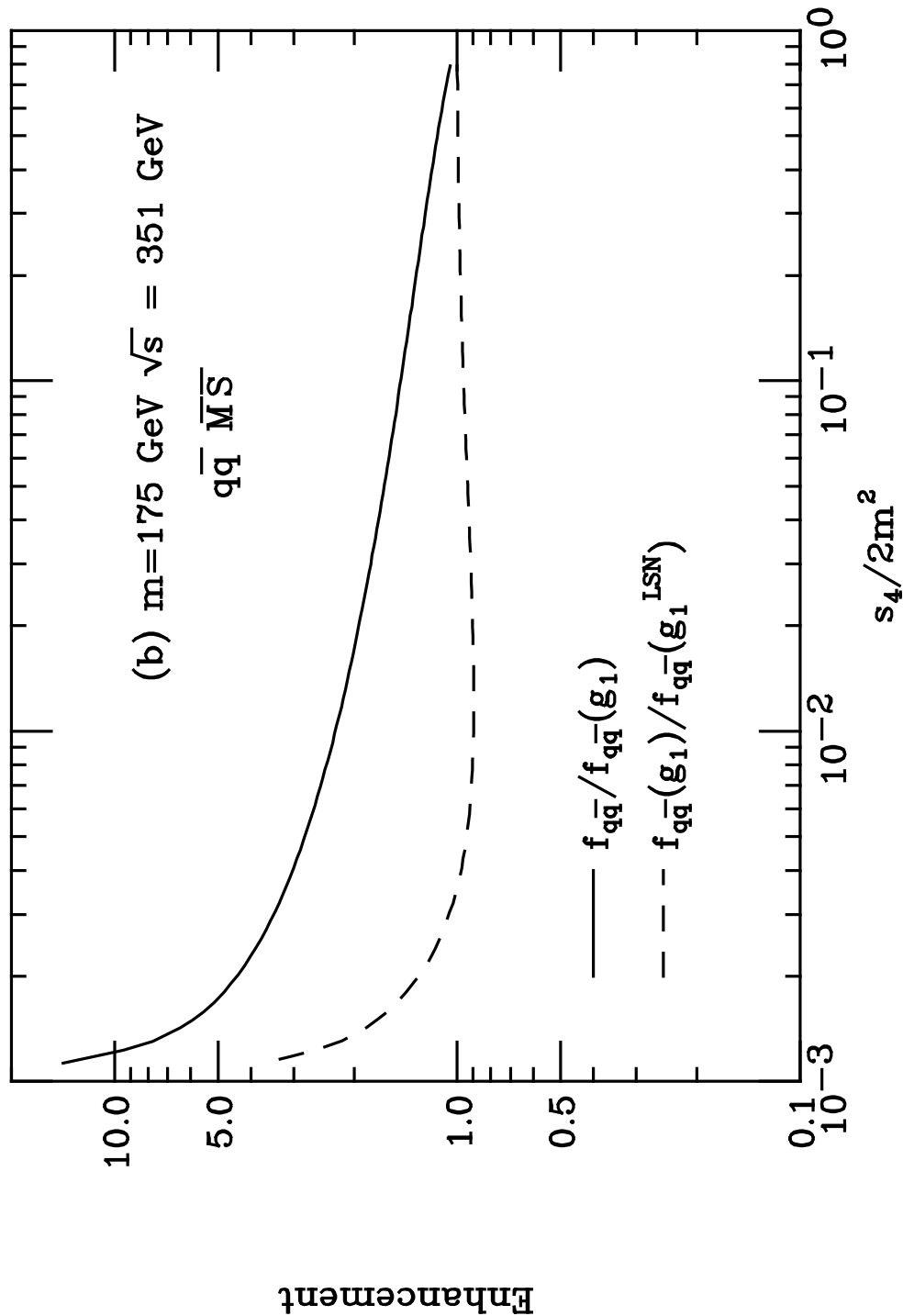


Figure 3

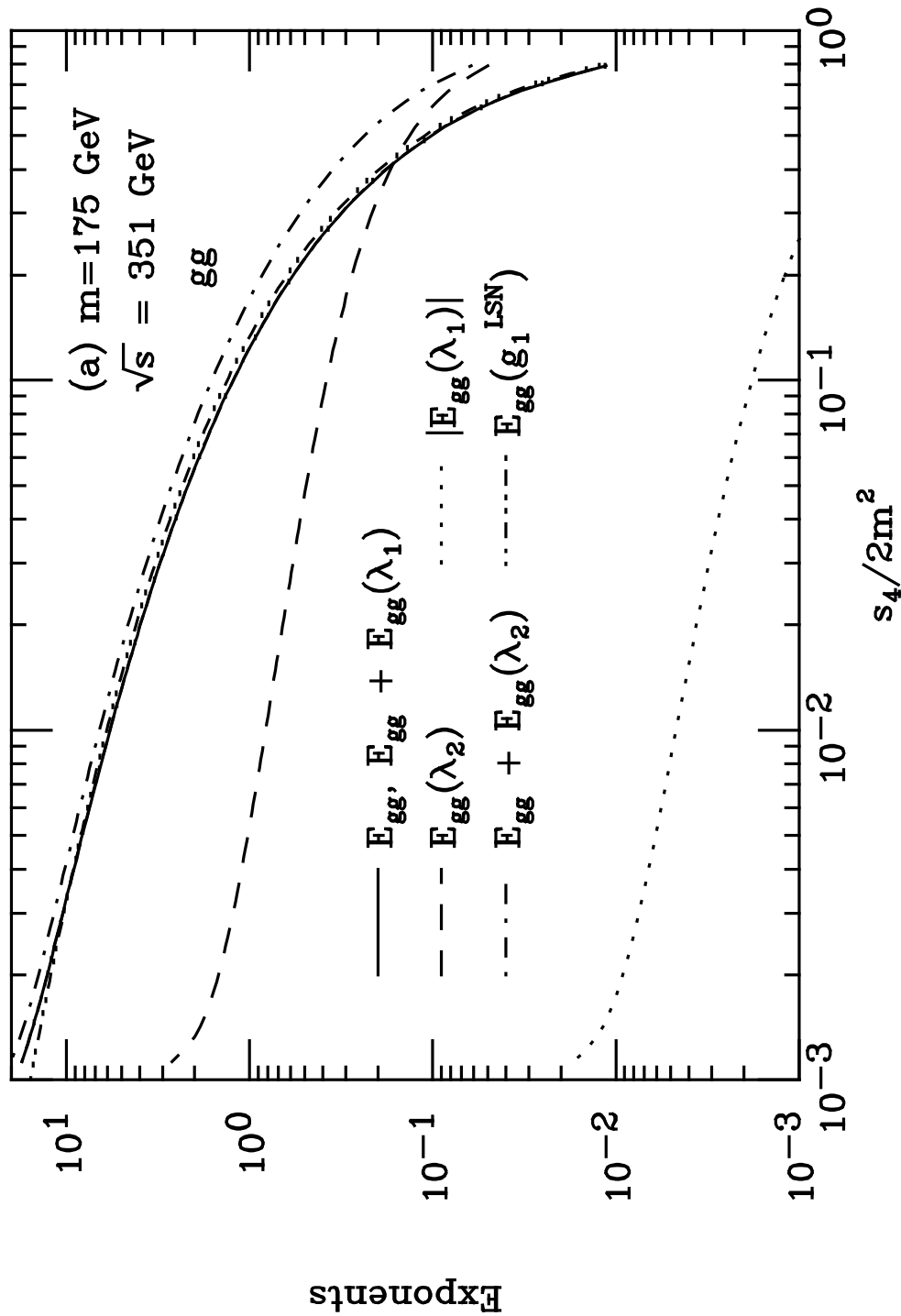


Figure 3

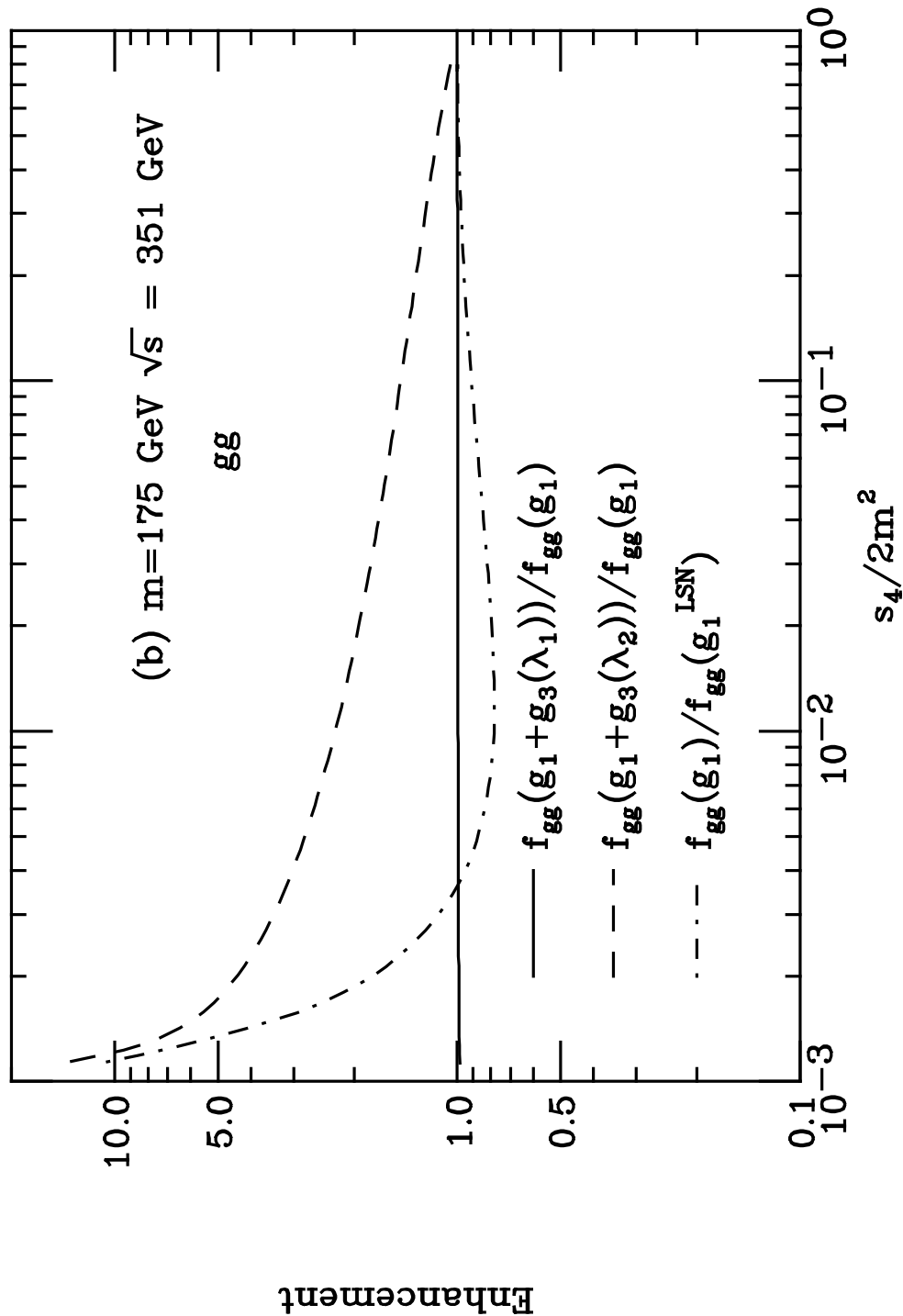


Figure 4

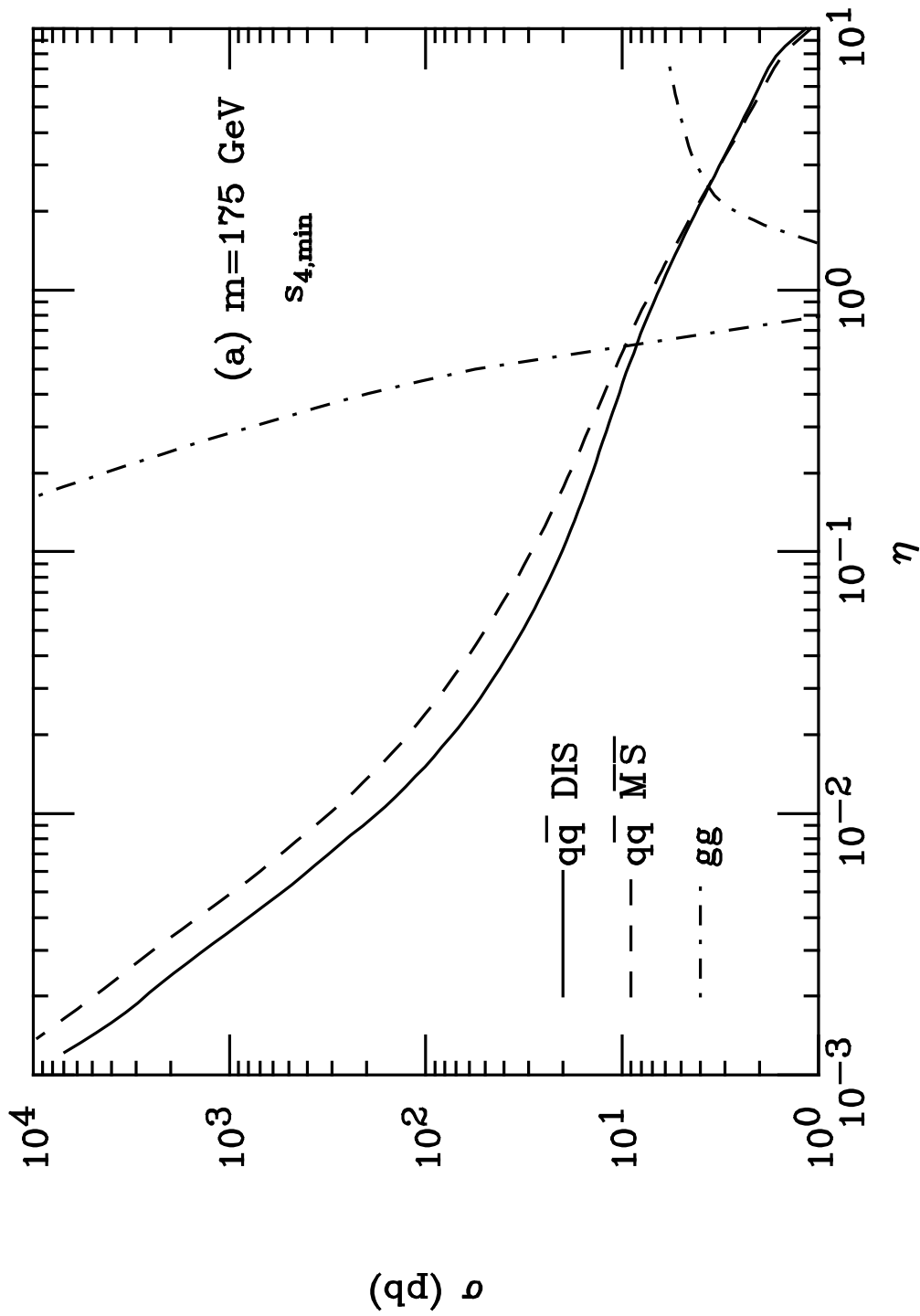


Figure 4

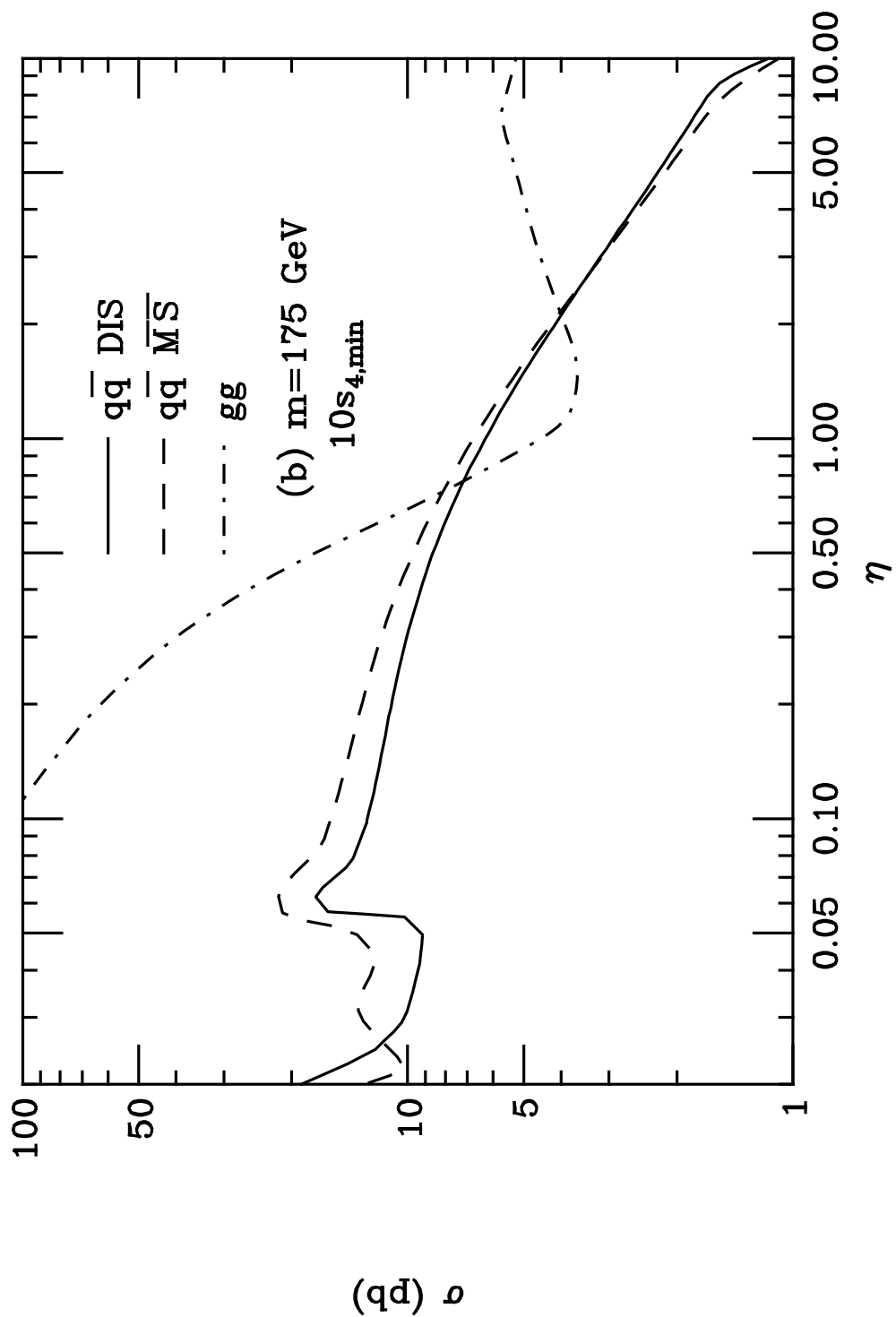


Figure 4

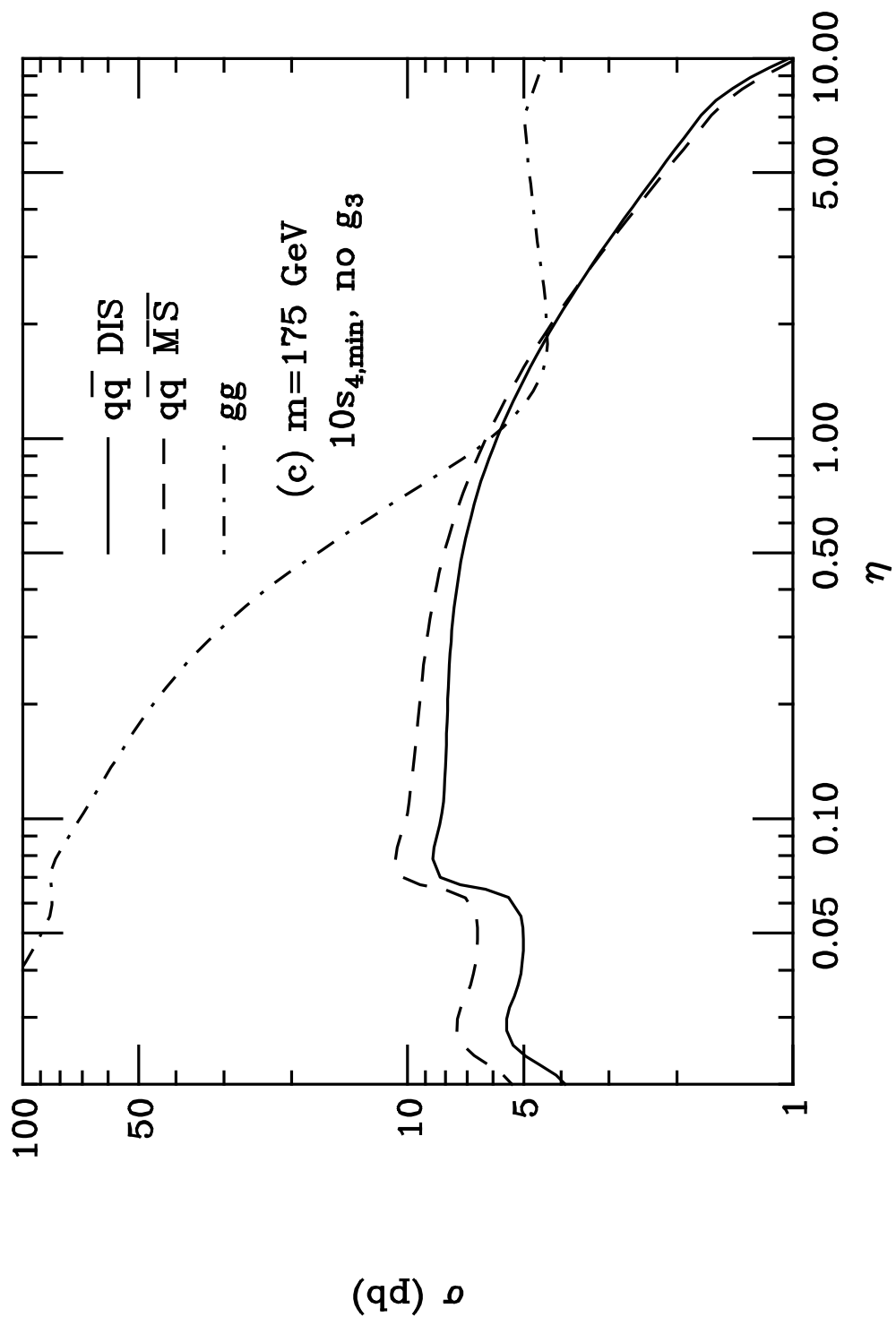


Figure 5

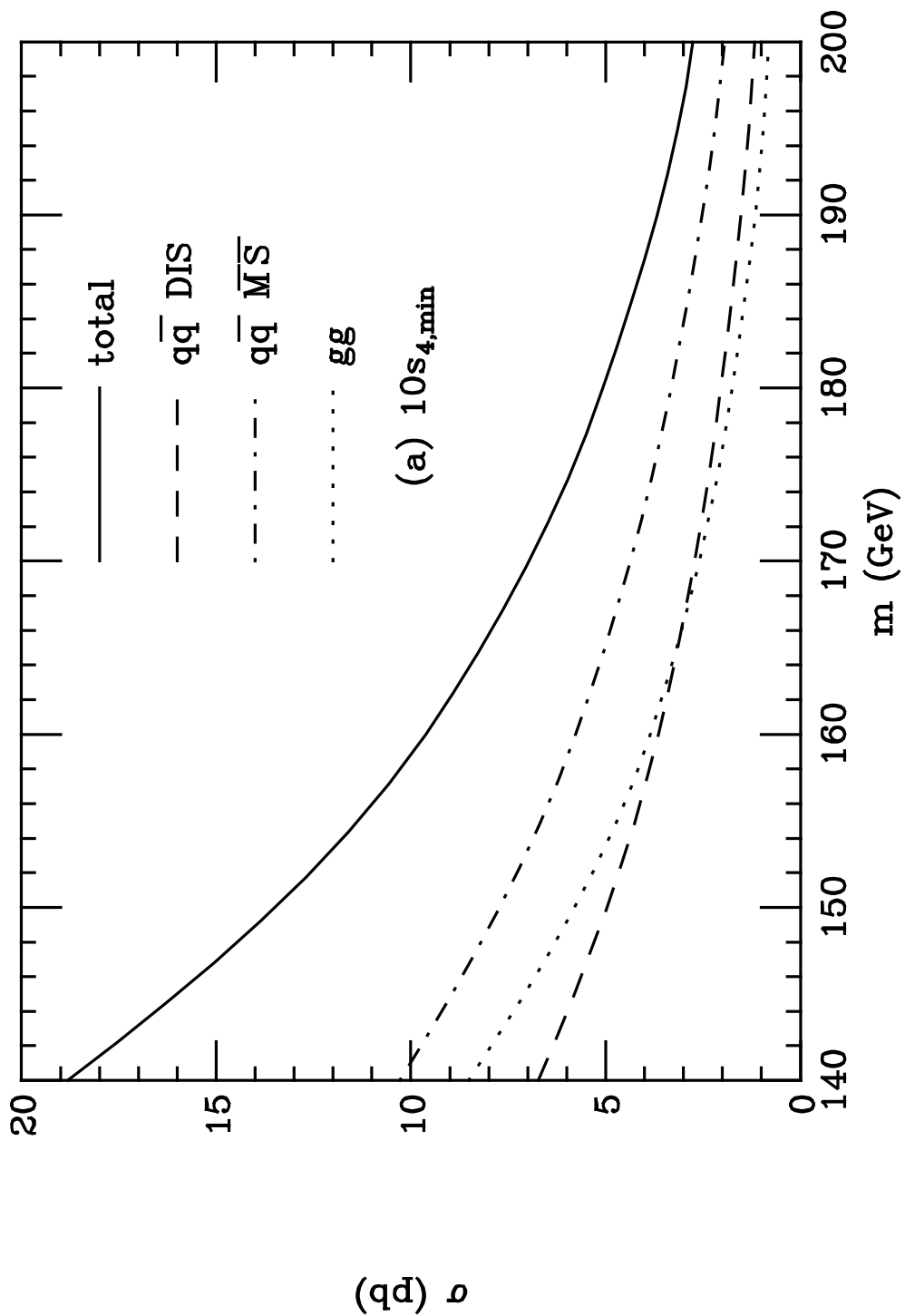


Figure 5

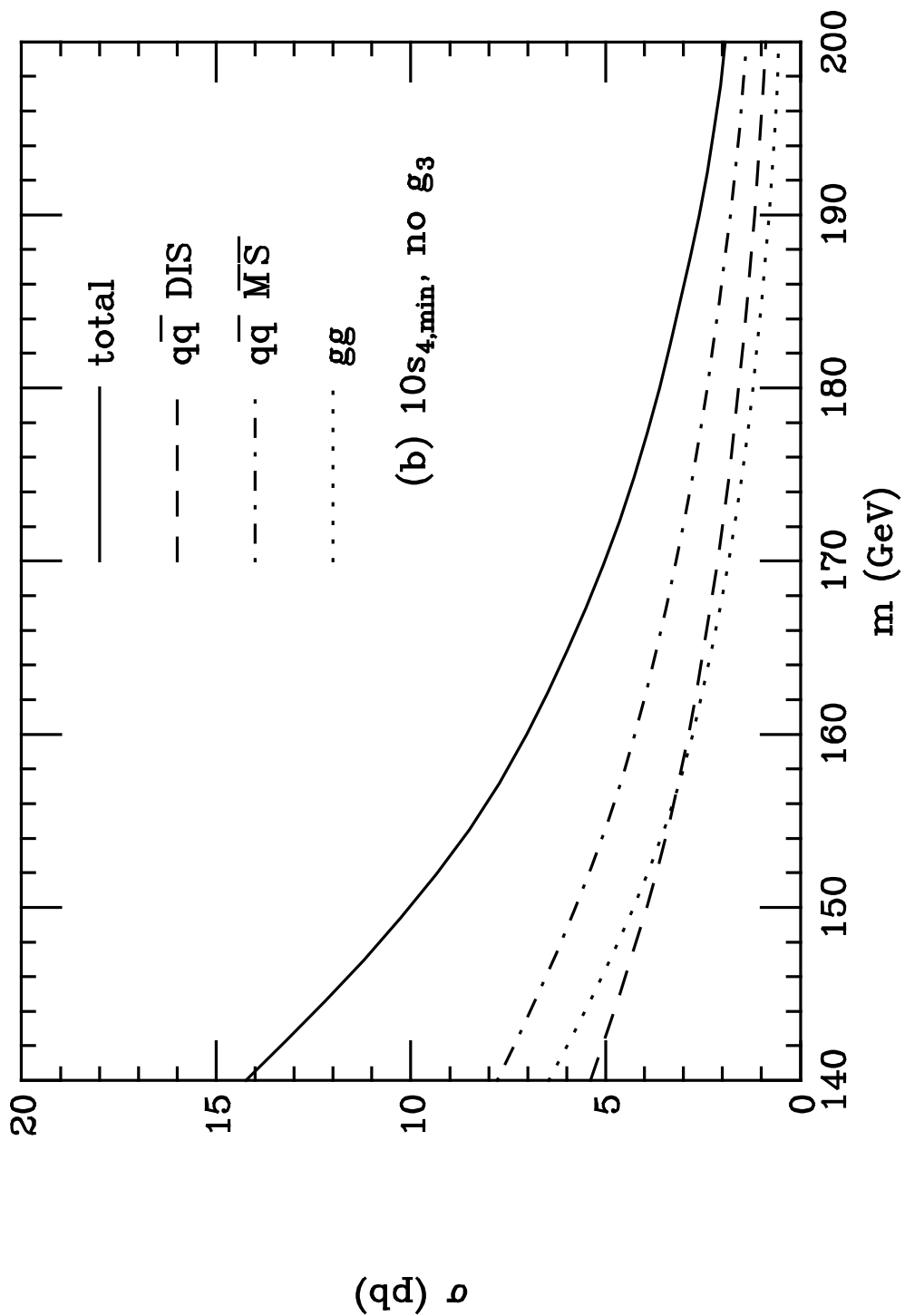


Figure 6

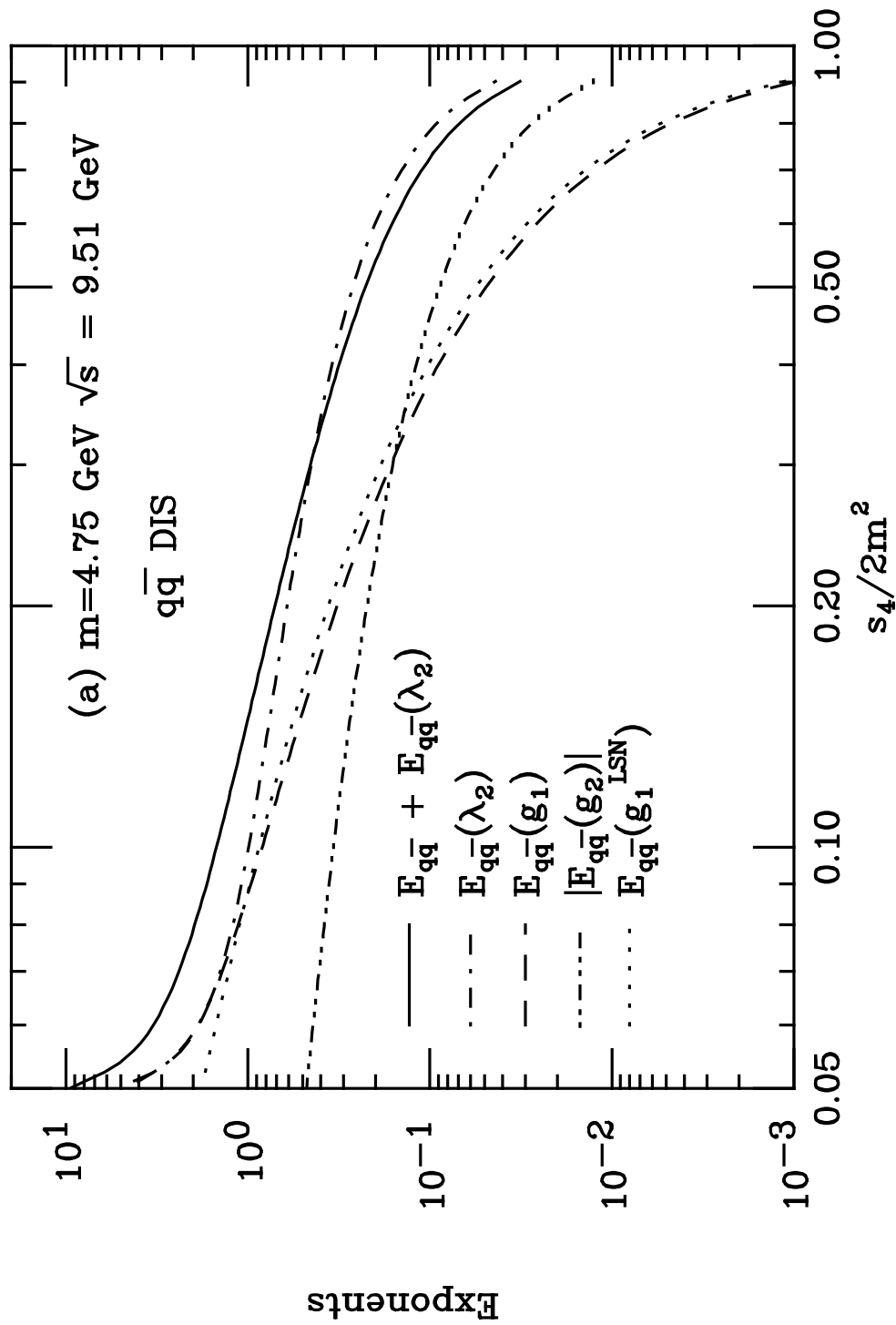


Figure 6

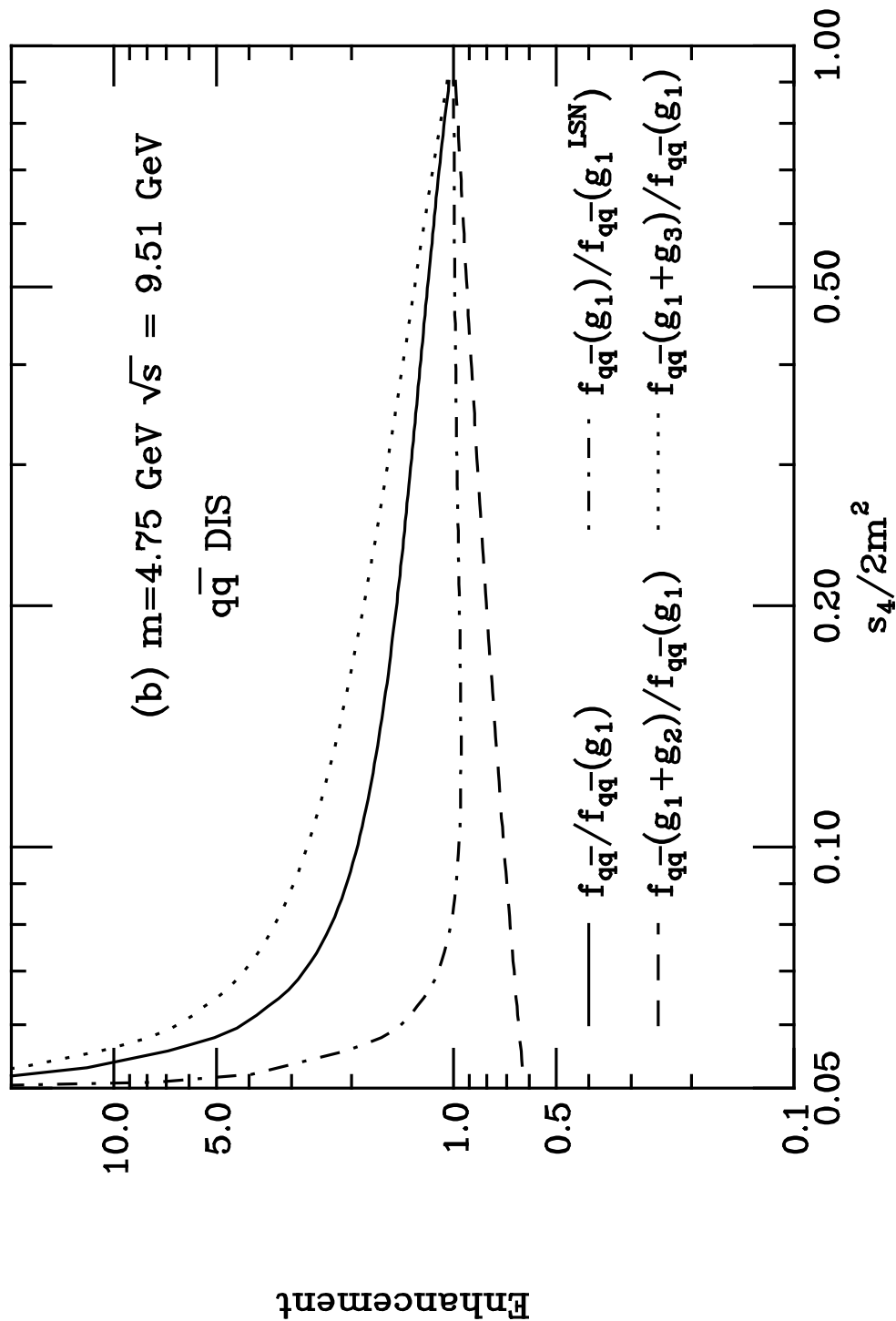


Figure 7

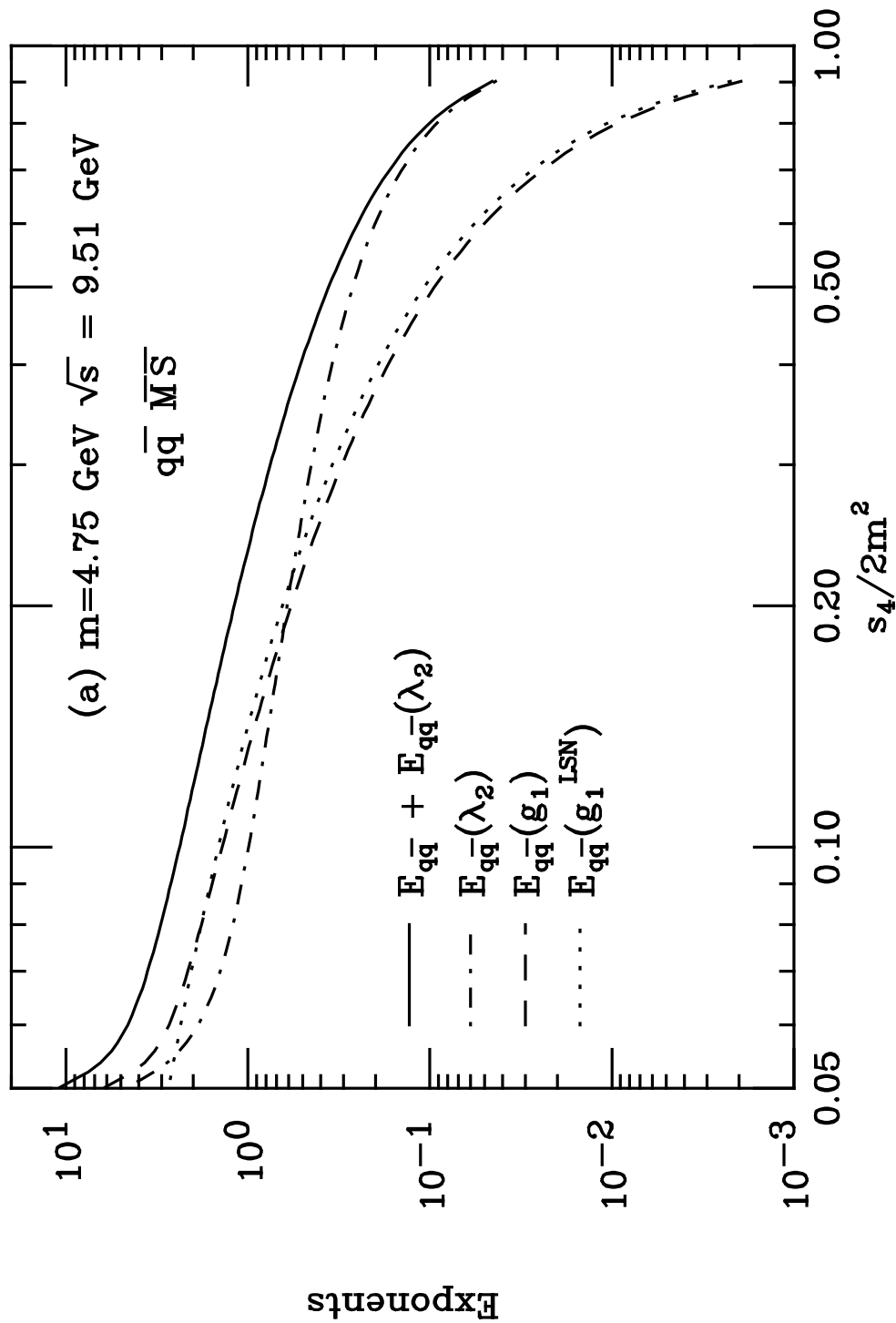


Figure 7

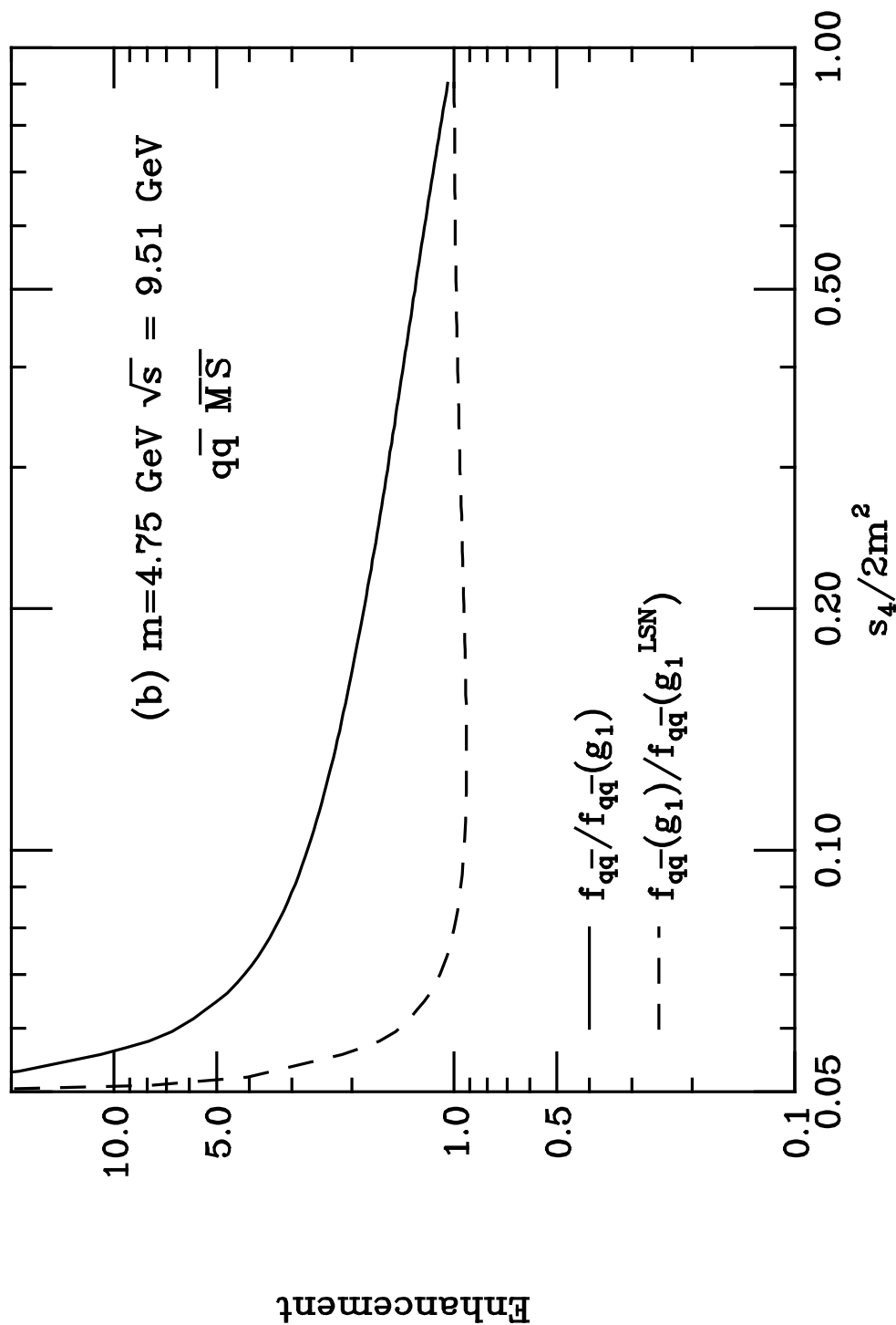


Figure 8

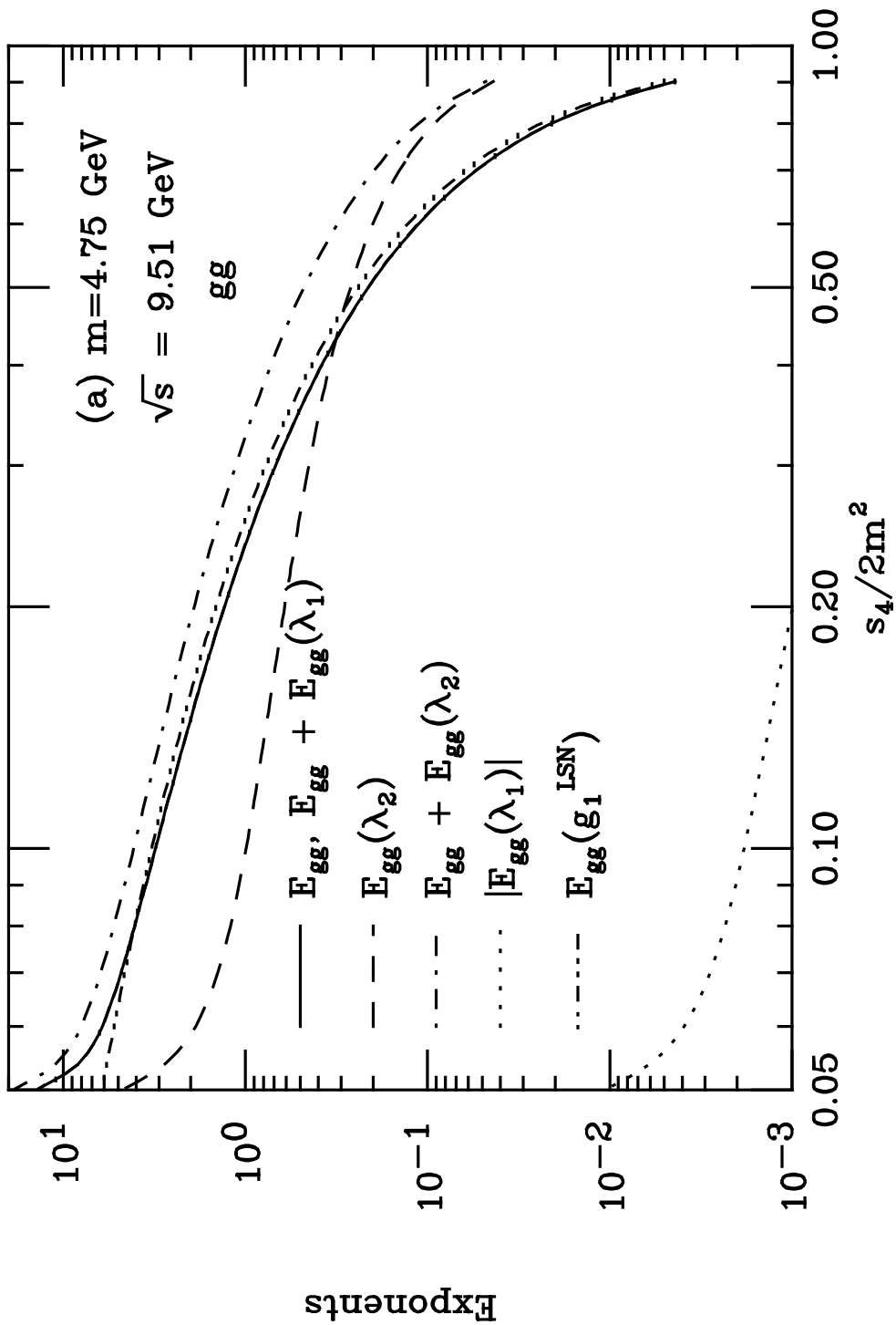


Figure 8

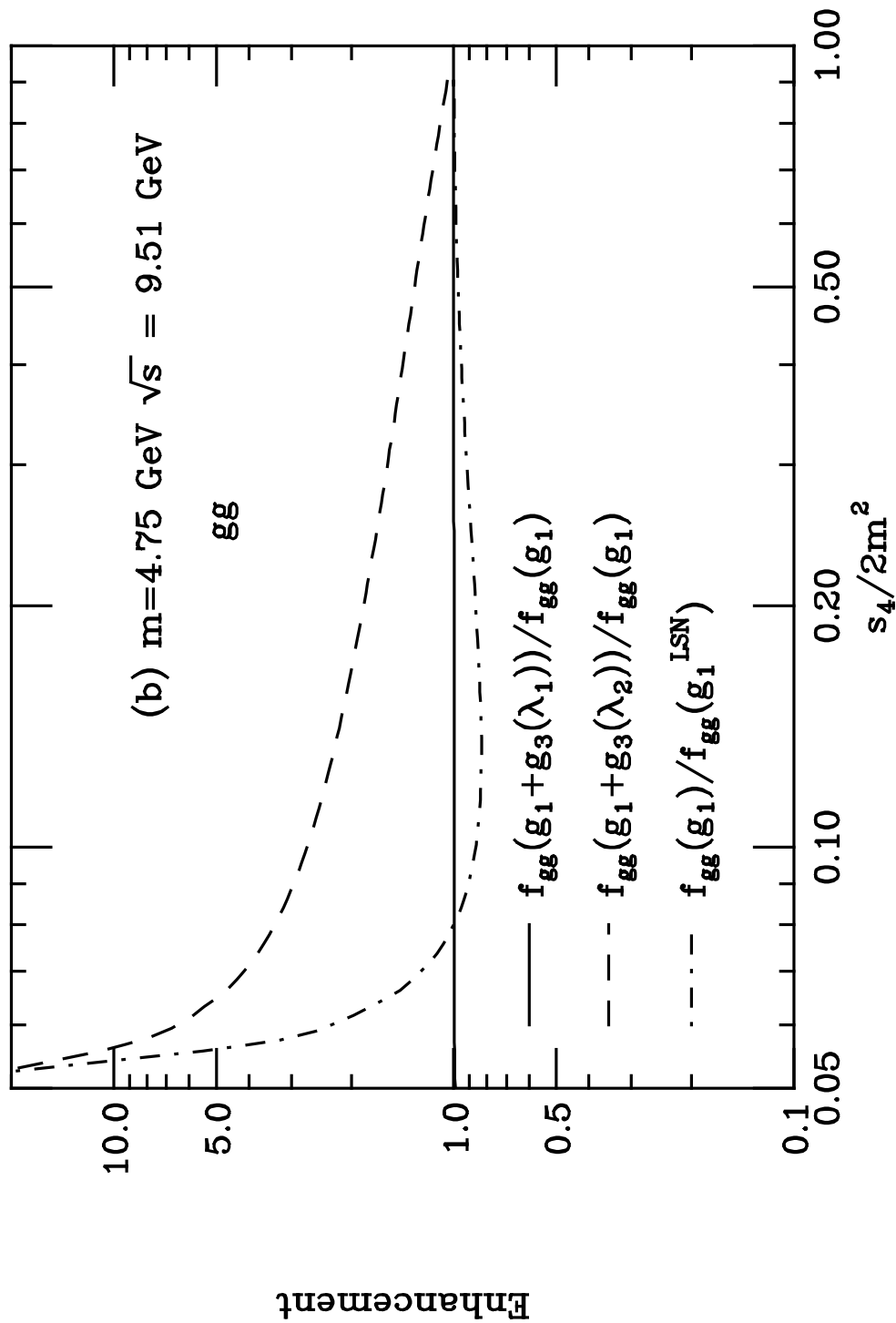


Figure 9

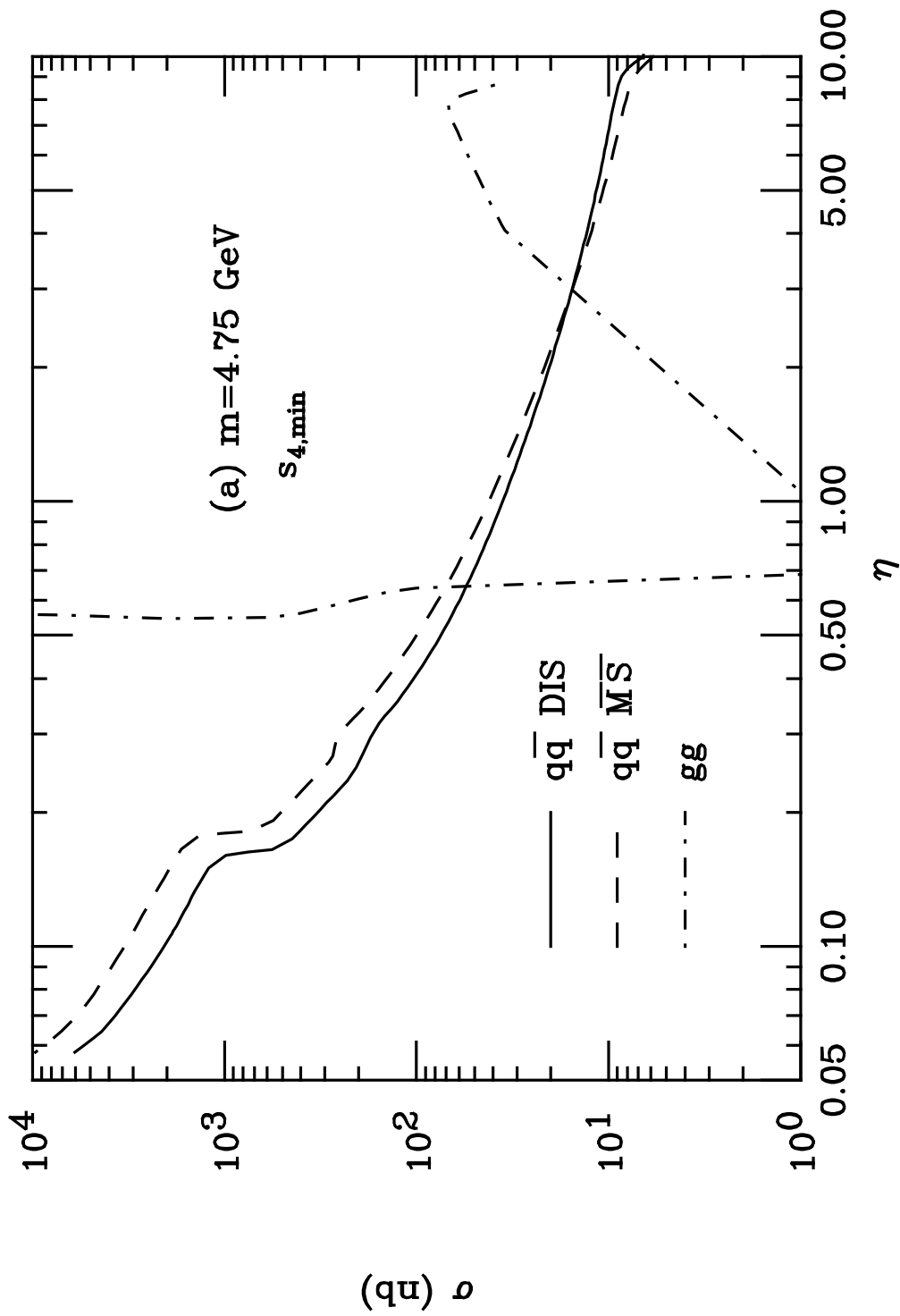


Figure 9

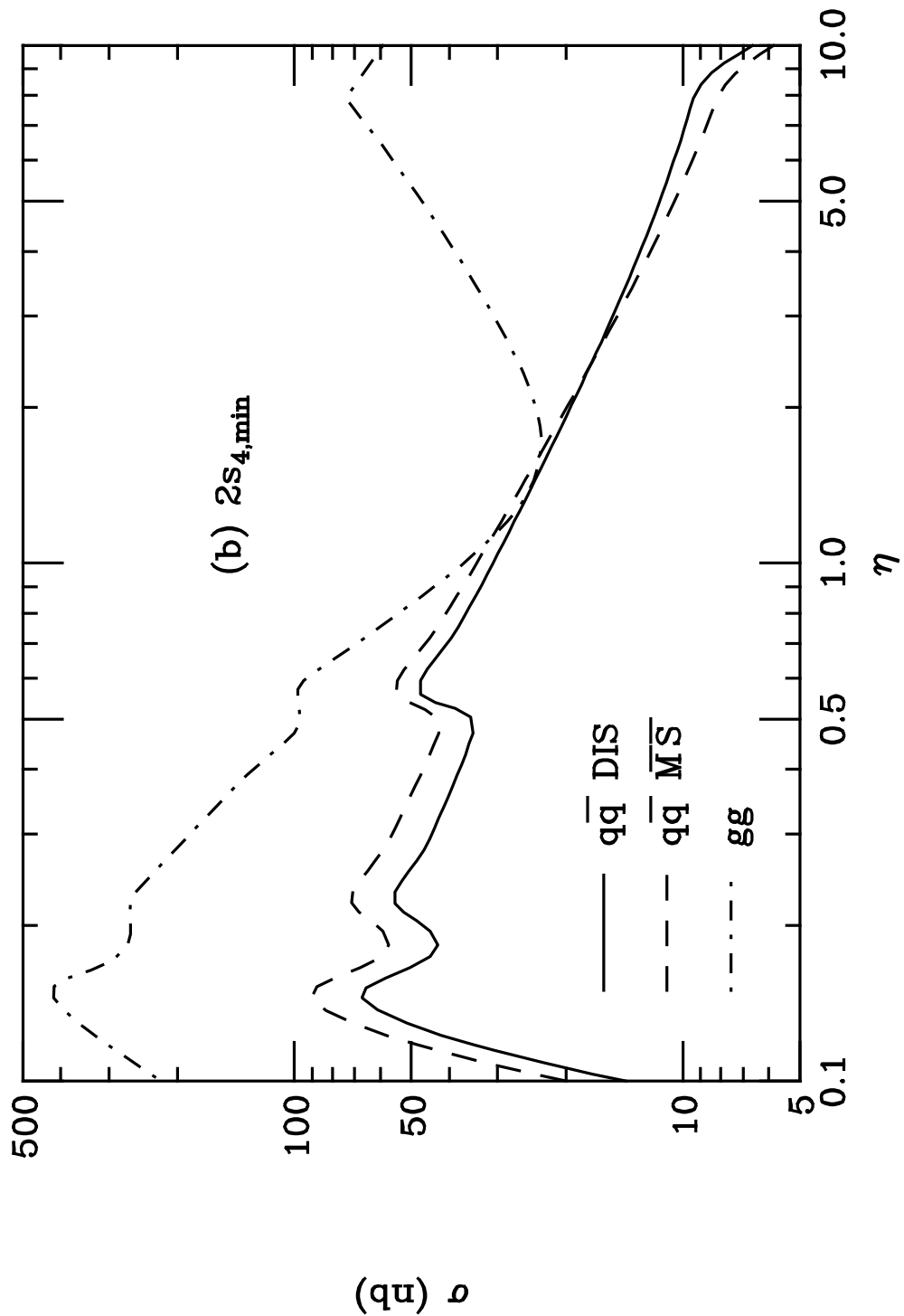


Figure 9

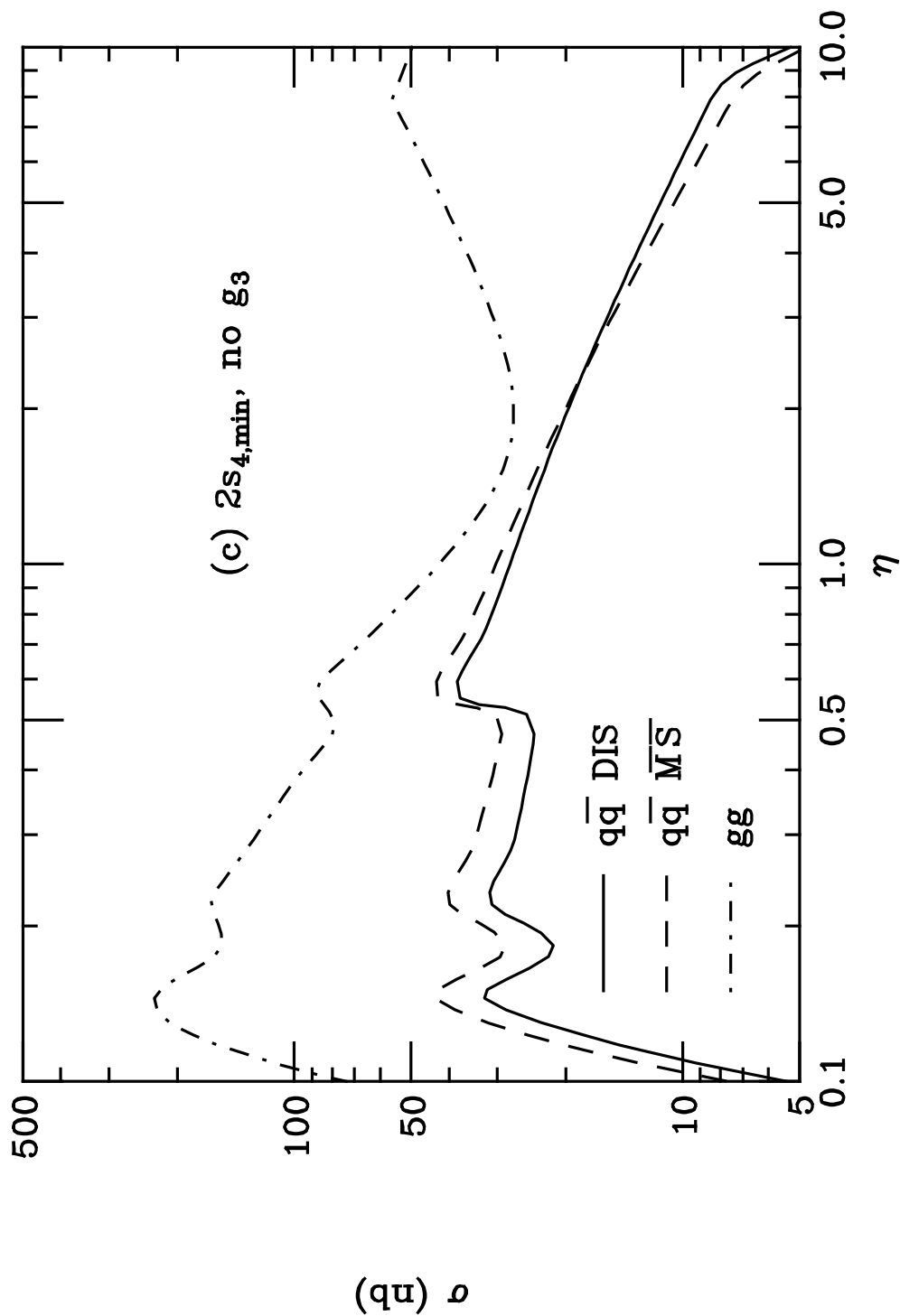


Figure 10

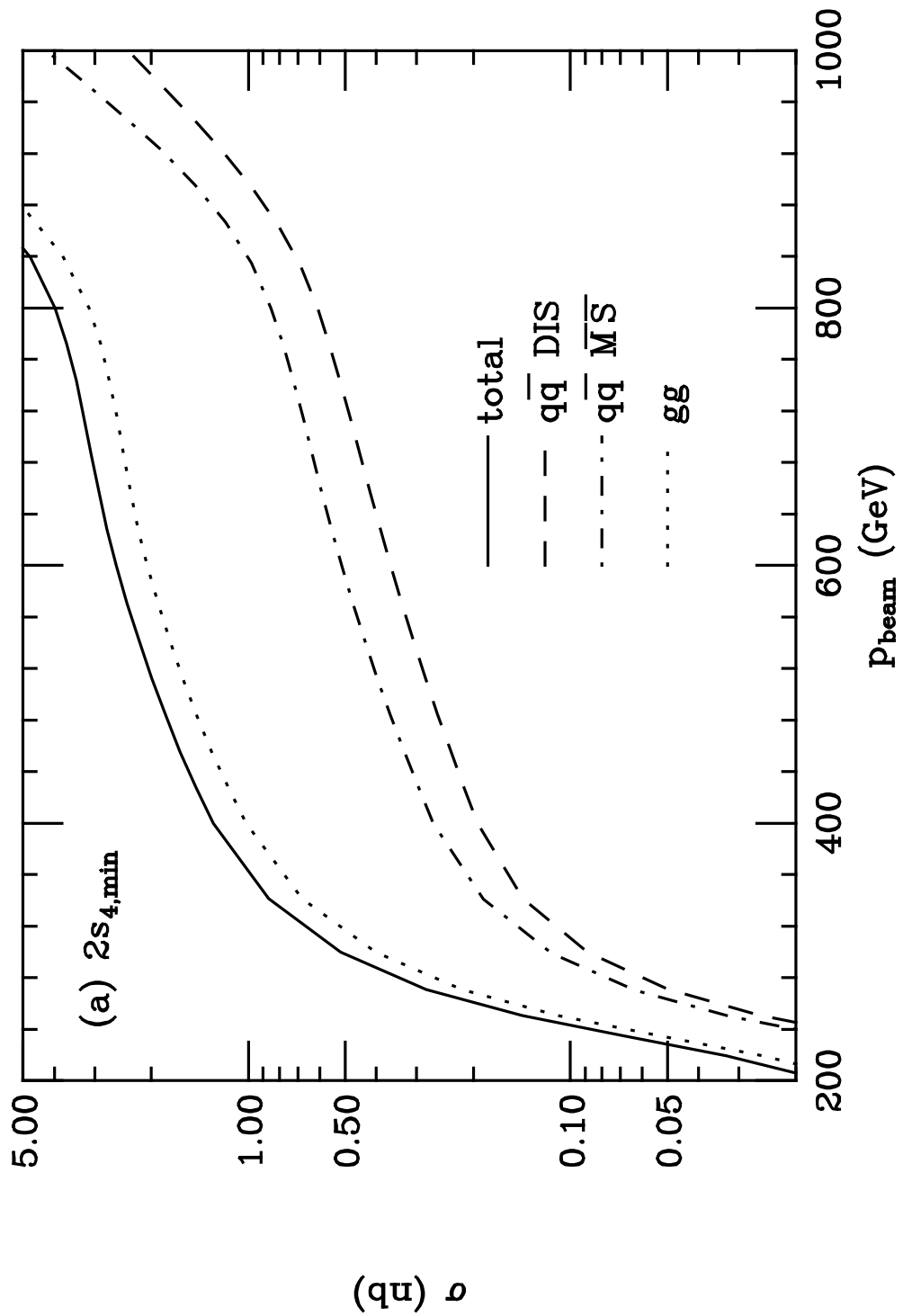


Figure 10

